Hindawi Publishing Corporation
Journal of Nanomaterials
Volume 2012, Article ID 624520, 22 pages
doi:10.1155/2012/624520

Review Article

Synthesis, Characterization, and Applications of ZnO Nanowires

Yangyang Zhang, Manoj K. Ram, Elias K. Stefanakos, and D. Yogi Goswami

Clean Energy Research Center, College of Engineering, University of South Florida, Tampa, FL 33620, USA

Correspondence should be addressed to Elias K. Stefanakos, estefana@usf.edu

Received 13 January 2012; Accepted 18 April 2012

Academic Editor: Tong Lin

ZnO nanowires (or nanorods) have been widely studied due to their unique material properties and remarkable performance in electronics, optics, and photonics. Recently, photocatalytic applications of ZnO nanowires are of increased interest in environmental protection applications. This paper presents a review of the current research of ZnO nanowires (or nanorods) with special focus on photocatalysis. We have reviewed the semiconducting photocatalysts and discussed a variety of synthesis methods of ZnO nanowires and their corresponding effectiveness in photocatalysis. We have also presented the characterization of ZnO nanowires from the literature and from our own measurements. Finally, a wide range of uses of ZnO nanowires in various applications is highlighted in this paper.

1. Introduction

Nanomaterials have attracted tremendous interest due to their noticeable performance in electronics, optics, and photonics. Nanomaterials are typically classified into three groups: 0-dimensional, 1-dimensional, and 2-dimensional. 0-dimensional nanostructures, referred to as quantum dots or nanoparticles with an aspect ratio near unity, have been extensively used in biological applications [1, 2]. 2-dimensional nanomaterials, such as thin films, have also been widely used as optical coatings, corrosion protection, and semiconductor thin film devices. One-dimensional (1D) semiconductor nanostructures such as nanowires, nanorods (short nanowires), nanofibres, nanobelts, and nanotubes have been of intense interest in both academic research and industrial applications because of their potential as building blocks for other structures [3]. 1D nanostructures are useful materials for investigating the dependence of electrical and thermal transport or mechanical properties on dimensionality and size reduction (or quantum confinement) [4]. They also play an important role as both interconnects and functional units in the fabrication of electronic, optoelectronic, electrochemical, and electromechanical nanodevices [5]. Among the one-dimensional (1D) nanostructures, zinc oxide (ZnO) nanowire is one of the most important nanomaterials for nanotechnology in today's research [6].

ZnO is a semiconductor material with a direct wide band gap energy (3.37 eV) and a large exciton binding energy (60 meV) at room temperature [7]. ZnO is also biocompatible, biodegradable, and biosafe for medical and environmental applications [8]. ZnO crystallizes in two main forms, hexagonal wurtzite and cubic zinc blende. Under general conditions, ZnO exhibits a hexagonal wurtzite structure. The crystalline nature of ZnO could be indexed to known structures of hexagonal ZnO, with $a = 0.32498$ nm, $b = 0.32498$ nm, and $c = 5.2066$ nm (JCPS card no. 36–1451) [9]. The ratio of c/a of about 1.60 is close to the ideal value for a hexagonal cell $c/a = 1.633$ [10]. The structure of ZnO could be described as a number of alternating planes composed of tetrahedrally coordinated O^{2-} and Zn^{2+} stacked alternately along the c-axis (Figure 1(a)). The O^{2-} and Zn^{2+} form a tetrahedral unit, and the entire structure lacks central symmetry (Figure 1(b)). Due to their remarkable performance in electronics, optics, and photonics, ZnO nanowires are attractive candidates for many applications such as UV lasers [11], light-emitting diodes [12], solar cells [13], nanogenerators [14], gas sensors [15], photodetectors

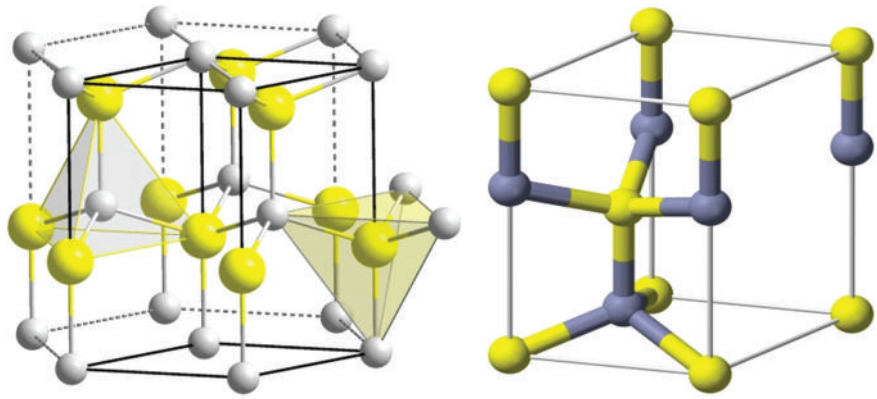

(a) (b)

Figure 1: ZnO structure: (a) the wurtzite structure model; (b) the wurtzite unit cell (from http://www.wikipedia.org/).

[16], and photocatalysts [17]. Among these applications, ZnO nanowires are being increasingly used as photocatalysts to inactivate bacteria and viruses and for the degradation of environmental pollutants such as dyes, pesticides, and volatile organic compounds under appropriate light irradiation [18, 19].

This paper reviews recent research in ZnO nanowires (or nanorods) with an emphasis on ZnO nanowires used in photocatalysis. In the following sections we have reviewed different semiconductor photocatalysts, compared their properties, and discussed a variety of synthesis methods of ZnO nanowires. We have also presented the characterization of ZnO nanowires from both the literature and our own measurements. Finally, a wide range of ZnO nanowires in various applications is highlighted in this paper.

2. Photocatalysts

Photocatalysis is a promising process for environmental protection because it is able to oxidize low concentrations of organic pollutants into benign products [20–26]. Photocatalysis utilizes semiconductor photocatalysts to carry out a photo-induced oxidation process to break down organic contaminants and inactivate bacteria and viruses [27–29]. Figure 2 illustrates the process of photocatalysis. When photons with energies greater than the band gap energy of the photocatalyst are absorbed, the valence band (VB) electrons are excited to the conduction band to facilitate a number of possible photoreactions. The photocatalytic surface with sufficient photo energy leads to the formation of a positive hole (h^+) in the valence band and an electron (e^-) in the conduction band (CB). The positive hole could either oxidize organic contaminants directly or produce very reactive hydroxyl radicals ($OH^\bullet$). The hydroxyl radicals ($OH^\bullet$) act as the primary oxidants in the photocatalytic system [30], which oxidize the organics. The electron in the conduction band reduces the oxygen that is adsorbed on the photocatalyst.

There are a number of semiconductors that could be used as photocatalysts, such as TiO_2, ZnO, and WO_3, Fe_2O_3. The

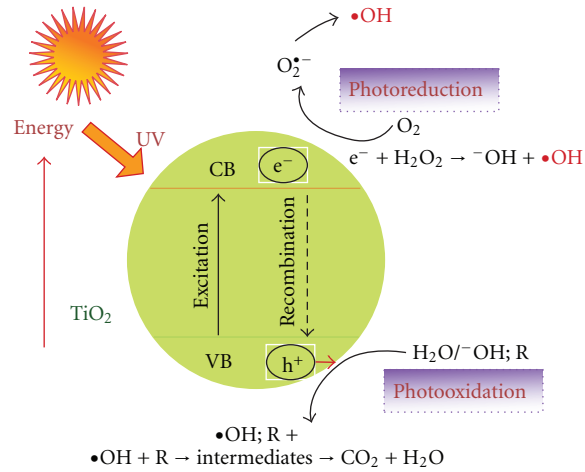

Figure 2: A schematic of the principle of photocatalysis (reproduced with permission from [30] ©2010 Elsevier).

band gap energy plays a significant role in the photocatalytic process. Figure 3 shows the band gap energies and the band edge positions of common semiconductor photocatalysts [31–33]. It is necessary to point out that the band gap values of ZnO, reported in the literature, are not all equivalent due to the different levels of the O vacancy in ZnO [34]. Although TiO_2 is the most widely investigated photocatalyst, ZnO has also been considered as a suitable alternative of TiO_2 because of its comparability with TiO_2 band gap energy and its relatively lower cost of production [18, 35, 36]. Moreover, ZnO has been reported to be more photoactive than TiO_2 [37–40] due to its higher efficiency of generation and separation of photoinduced electrons and holes [18, 41, 42].

Since the contaminant molecules need to be adsorbed on the photocatalytic surface before the reactions take place, the surface area plays a significant role in the photocatalytic activity. Although nanoparticles offer a large surface area, they have mostly been used in water suspensions, which limit their practical use due to difficulties in their

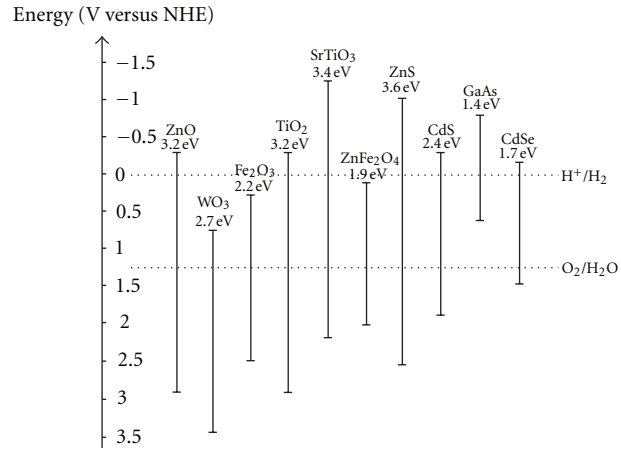

Figure 3: Band edge positions of common semiconductor photocatalysts (data from [32, 33, 43]).

separation and recovery. Moreover, additional equipment is needed for catalyst nanoparticle separation. Photocatalyst supported on a steady substrate can eliminate this issue. One-dimensional nanostructures, such as nanowires grown on a substrate, offer enhanced photocatalytic efficiency due to their extremely large surface-to-volume ratio as compared to a catalyst deposition on a flat surface [28, 44]. Table 1 compares different ZnO nanostructures for photocatalytic applications. There are many advantages in nanowire structures that could be used as photocatalysts.

3. Synthesis of ZnO Nanowires

ZnO nanowires can be either grown independently or grown on certain substrates. However, a vertical aligned growth on a substrate has more advantages in photocatalytic applications. The anisotropy of the ZnO crystal structure assists the growth of nanowires. The most common polar surface is the basal plane (0 0 1) with one end of the basal polar plane terminating in partially positive Zn lattice points and the other end terminating in partially negative oxygen lattice points. The anisotropic growth of the nanowires takes place along the *c*-axis in the [0 0 0 2] direction [45]. The growth velocities under hydrothermal conditions along the different directions are following the pattern $V(0001) > V(1011) > V(1010)$ [46]. The relative growth rate of these crystal faces will determine the final shape and aspect ratio of the ZnO nanostructures.

The synthesis methods of ZnO nanowires could mainly be classified as vapor phase and solution phase synthesis.

3.1. The Vapor Phase Synthesis. Vapor phase synthesis is probably the most extensively explored approach in the formation of 1D nanostructures [5]. A typical vapor phase synthesis method takes place in a closed chamber with a gaseous environment. Vapor species are first produced by evaporation, chemical reduction, and gaseous reaction. After that, the species are transferred and condensed onto the surface of a solid substrate. Generally, the vapor phase synthesis process is carried out at higher temperatures from 500°C to 1500°C and produces high-quality nanowires. The typical vapor phase synthesis method includes vapor liquid solid (VLS) growth [47], chemical vapor deposition (CVD) [48], metal organic chemical vapor deposition (MOCVD) [49], physical vapor deposition (PVD) [50], molecular beam epitaxy (MBE) [51], pulsed laser deposition (PLD) [52], and metal organic vapor phase epitaxy (MOVPE) [53]. Among the vapor phase synthesis methods, VLS and MOCVD are two of the most important methods for the ZnO nanowires synthesis.

Compared to other vapor phase techniques, VLS method is a simpler and cheaper process, and is advantageous for growing ZnO on large wafers [54]. The VLS process has been widely used for the growth of 1D nanowires and nanorods. A typical VLS process is used with nanosized liquid metal droplets as catalysts. The gaseous reactants interact with the nanosized liquid facilitating nucleation and growth of single crystalline rods and wires under the metal catalyst. Typical metal catalysts in the VLS process are Au, Cu, Ni, Sn, and so forth. ZnO nanowires have been successfully grown on sapphire, GaN, AlGaN, and ALN substrates through the VLS process [55]. The quality and growth behavior of the ZnO nanowires are strongly affected by the chamber pressure, oxygen partial pressure, and thickness of the catalyst layer [56, 57]. Chu et al. [58] synthesized well-aligned ZnO nanowires using VLS mechanism on Si substrate with chamber temperature varying from 600 to 950°C and pressure from 0.75 to 3 torr. They showed that ZnO nanowires with high aspect ratio grew vertically on the substrate at 700 to 750°C, the density of nanowires decreased when the temperature was higher than 800°C, and the growth rate and length of nanowires were decreased with increasing total chamber pressure.

Catalyst-free metal-organic chemical vapor deposition (MOCVD) is another important synthesis method for ZnO nanowires [49, 59]. The catalyst-free method eliminates the possible incorporation of catalytic impurities and produces high-purity ZnO nanowires. Moreover, the growth temperature of catalyst-free MOCVD is lower than a typical VLS growth temperature [60]. The ability to grow high-purity ZnO nanowires at low temperatures is expected to greatly increase the versatility and power of these building blocks for nanoscale photonic and electronic device applications [5]. Zeng et al. [61] reported that well-aligned ZnO nanowires were prepared by MOCVD on Si substrate without catalysts. In their grown process, high-purity diethyl zinc (99.999%) and N_2O (99.999%) were used as zinc and oxygen sources, respectively, and N_2 as the carrier gas. The base pressure of the reactor chamber and the working pressure were 10^{-5} and 50 torr, respectively. A thin nucleation layer of ZnO was grown at a low substrate temperature of 400°C at the beginning. After annealing the nucleation layer, ZnO nanowires were grown on the nucleation layer at the substrate temperature of 650°C.

Physical vapor deposition (PVD) technique has also been used to fabricate ZnO nanowires. The advantages of PVD technique are the following: (1) composition of products can be controlled, (2) there is no pollution such as drain

Table 1: Comparison of different ZnO nanostructures used in photocatalytic applications.

Nanoparticles		Nanowires		Nanothin film	
Advantages	Disadvantages	Advantages	Disadvantages	Advantages	Disadvantages
Could be suspended in a solution	Particle aggregation in a solution leads to a reduced surface area	Growth could be well aligned on most substrates	Growth conditions are more restricted	Coated on certain substrates	Lower performance because of small surface area
High performance because of larger surface areas	Posttreatment for catalyst removal is required	Offer larger surface area compared to nanothin film	Lower surface area compared to nanoparticles	Posttreatment for catalyst removal is not required	
	Difficult to recover all the catalyst	Posttreatment for catalyst removal is not required			
		Lower crystallinity and more defects			

water, discharge gas, and waste slag, and (3) simple process of making samples [62]. The process of PVD usually is direct thermal evaporation and oxidation of Zn powder at a high temperature and then deposition on the substrate to form the final product [50]. Zhang et al. [62] demonstrate the fabrication of ZnO nanowire arrays on Si substrates by PVD method at a relatively low temperature of about 500°C. In their synthesis process, high-purity Zn powder as source material was placed in a ceramic boat located at the center of a horizontal tube furnace. The Si substrates were placed on top of the boat to collect the products. The system was quickly heated to 500°C under 50 cm^3/min N_2 flowing at a pressure of about 10^{-3} torr for 1 h and then cooled to room temperature. The optical investigation showed that the ZnO nanowires were of high crystal quality and had attractive optical properties.

3.2. Solution Phase Synthesis. Solution phase synthesis has many advantages when compared to vapor phase synthesis, such as low cost, low temperature, scalability, and ease of handling. Generally, solution phase reactions occur at relatively low temperatures (<200°C) compared to vapor phase synthesis methods. Thus, solution synthesis methods allow for a greater choice of substrates including inorganic and organic substrates. Due to the many advantages, solution phase synthesis methods have attracted increasing interest. In solution phase synthesis, the growth process could be carried out in either an aqueous or organic solution or a mixture of the two [63, 64].

3.2.1. Hydrothermal Method. Generally, solution phase synthesis is carried out in an aqueous solution, and the process is then referred to as the hydrothermal growth method [65, 66]. Hydrothermal methods have received a lot of attention and have been widely used for synthesis of 1D nanomaterials. In addition, hydrothermally grown ZnO nanowires have more crystalline defects than others primarily due to oxygen vacancies [28]. Nanowires with inherent defects are capable of exhibiting visible light photocatalysis even without doping with transition metals [67]. The general process for vertically aligned ZnO nanowires grown on a substrate by the hydrothermal method is the following.

(a) A thin layer of ZnO nanoparticles is seeded on a certain substrate. The seeding layer promotes nucleation for the growth of nanowires due to the lowering of the thermodynamic barrier [68].

(b) An alkaline reagent (such as NaOH or hexamethylenetetramine) and Zn^{2+} salt ($Zn(NO_3)_2$, $ZnCl_2$, etc.) mixture aqueous solution is used as a precursor (or growth solution).

(c) The ZnO seeded substrate is kept in the growth solution at a certain temperature and a certain period of time.

(d) The resultant substrate and growth layer is washed and dried.

When hexamethylenetetramine ($(CH_2)_6N_4$, or HTMA) and $Zn(NO_3)_2$ are chosen as precursor, the chemical reactions can be summarized in the following equations [35]

Decomposition reaction:

$$(CH_2)_6N_4 + 6H_2O \longrightarrow 6HCHO + 4NH_3 \quad (1)$$

Hydroxyl supply reaction:

$$NH_3 + H_2O \longleftrightarrow NH_4^+ + OH^- \quad (2)$$

Supersaturation reaction:

$$2OH^- + Zn^{2+} \longrightarrow Zn(OH)_2 \quad (3)$$

ZnO nanowire growth reaction:

$$Zn(OH)_2 \longrightarrow ZnO + H_2O \quad (4)$$

One of the key parameters for the growth of ZnO nanowires is controlling the supersaturation of the reactants. It is believed that high supersaturation levels favor nucleation and low supersaturation levels favor crystal growth [3]. If a lot of OH^- is produced in a short period, the Zn^{2+} ions in the solution will precipitate out quickly due to the high pH environment, and, therefore, Zn^{2+} would contribute little to the ZnO nanowire growth and eventually result in the fast consumption of the nutrient and prohibit further growth of the ZnO nanowires [69]. Thus, the concentration of OH^- should be controlled in the solution to maintain low supersaturation levels during the whole nanowire growth process.

Effect of the ZnO Seeding Layer. Typical preseeding methods include thermal decomposition of zinc acetate, spin coating of ZnO nanoparticles, sputter deposition, and physical vapor deposition. In order to seed ZnO particles on the substrate, ZnO seeds must be annealed at certain temperature to improve ZnO particle adhesion to the substrate and nanowire vertical growth alignment. Greene et al. [70] studied the minimum temperature required to form textured seeds from zinc acetate on a silicon substrate from 100 to 350°C. The results suggest that temperatures between 150 and 200°C are needed for seed alignment, whereas higher temperatures promote seed crystallinity and growth. Baruah and Dutta [71] have reported that a very uniform thin layer of ZnO nanoparticles could be observed when ZnO seeds are annealed at a temperature of 350°C. However, when the annealing temperature was further increased to 450°C, ZnO crystallized into nanoparticles as well as nanorod-like structures. The authors hinted that ZnO seeds annealing at a temperature of about 350°C could give the best results for the ZnO nanowire growth.

The texture, thickness, and crystal size of ZnO seed layers also affect the quality of ZnO nanowire growth [72–75]. Ghayour et al. [72] reported the effect of seed layer thickness on alignment and morphology of ZnO nanorods. The results showed that the diameter increased, the density decreased, and the length of the nanorods slightly decreased when the thickness of the seed layer increased (Table 2). Wu et al. [73] studied the effects of seed layer characteristics on the synthesis of ZnO nanowires. The SEM images showed the density of nanowires decreased from 35 to 12 μm^{-2} when the thickness increased from 106 to 191 nm and the diameter of the nanowires was found to increase with the seed layer (002) grain size. Ji et al. [75] found that the average diameter of nanowires is increased from 50 to 130 nm and the density is decreased from 110 to 60 μm^{-2} when the seed layer thickness is changed from 20 to 1000 nm. Baruah and Dutta [71] reported that the nanorods grown on seeds crystallized from a zinc acetate solution have a higher aspect ratio (of the order of 3) than those grown using nanoparticle-seeded substrates.

Without a ZnO seeding layer, ZnO nanowires could be grown on an Au/substrate by introducing a suitable content of ammonium hydroxide into the precursor solution [76]. Au is used as an "intermediate layer" to assist the growth of ZnO nanowires [76].

Effect of an Alkaline Reagent. There are some alkaline reagents that have been used to supply OH^- during the reaction process such as NaOH, hexamethylenetetramine (HMTA), Na_2CO_3, ammonia, and ethylenediamine. When NaOH, KOH, or Na_2CO_3 is chosen, the synthesis process usually is carried out at elevated temperatures (>100°C) and pressures in a Teflon-sealed stainless autoclave [77–80]. When HMTA, ammonia, or ethylenediamine is chosen, the synthesis process can be carried out at lower temperatures (<100°C) and an atmospheric pressure. However, HMTA is the most often used due to its advantage in producing high-quality ZnO nanowires [81]. HMTA plays different significant roles during the synthesis process. First, HMTA supplies the OH^- ions to drive the precipitation reaction by thermal degradation [82]. Second, HMTA acts as a pH buffer by slowly releasing OH^- ions through thermal decomposition [81]. The hydrolysis rate of HMTA is decreased with an increase in pH and vice versa. Third, HMTA attaches to the nonpolar facets of the ZnO nanowires and prevents access of the Zn^{2+} ions to them thus leaving only the polar (001) face for epitaxial growth [68].

Effect of Precursor Concentration. To ascertain the relationship between the precursor concentration and the ZnO nanowire growth, Wang et al. [83] carried out a series of experiments by varying the precursor concentration and different ratios of $[Zn(NO_3)_2]/[C_6H_{12}N_4]$. The effect of the concentration of the precursor on the growth of ZnO nanorods is to increase the average diameter of ZnO nanorods almost linearly from 43 to 70 nm and the average length from 65 to 320 nm, as the precursor concentration increases from 0.008 to 0.04M (Figure 4). The corresponding aspect ratio of the ZnO nanorods increases from 1.8 to 5.8 and then slightly decreases to 4.6 (Figure 4 insert). Changes in the $[Zn(NO_3)_2]/[C_6H_{12}N_4]$ ratio did not have a significant effect on the diameters of the ZnO nanorods (Figure 5). The aspect ratio of the ZnO nanorod arrays reached a maximum value of 7.25 when the $[Zn(NO_3)_2]/[C_6H_{12}N_4]$ ratio was set to unity (Figure 5 insert). Xu et al. [69] studied the nanowire density by varying the precursor concentration with equal molar concentrations of the zinc salt and HMTA. The experimental results showed that the density of the nanowires is closely related with the precursor concentration. From 0.1 to 5 mM, the ZnO nanowire density was increased from 55/100 μm^2 to 108/100 μm^2. When the precursor concentration is further increased, the density of ZnO nanowires remains approximately steady with a slight decreasing tendency. The authors explained that the zinc chemical potential inside the body of the solution increases with zinc concentration. To balance the increased zinc chemical potential in the solution, more nucleation sites on the substrate surface will be generated, and, therefore, the density of the ZnO nanowires will increase. However, a continuous increase in the solution concentration may not increase the density of the nanowires when its density is larger than the saturation density. Kim et al. [84] reported that the density and diameter of ZnO nanorods are especially sensitive to the concentration of the reactants. Furthermore, the structural transition is shown by increasing the concentration. At the lowest concentration of Zn^{2+}, the ZnO nanorods grow as single crystals with a low density and variable orientations. On the other hand, at the highest concentration, the nanorods grow as polycrystals due to the supersaturated Zn^{2+} source.

Effect of Growth Duration Time. Yuan et al. [85] synthesized ZnO nanowires by using equimolar (50 mM) zinc nitrate and HMTA at 93°C. The authors reported that the average diameter of ZnO nanowires is increased with growth duration time when the growth time is less than 2.5 h (Table 3). However, the average diameter is almost

Table 2: The diameter, density, and length of ZnO nanorods corresponding to the thickness of the seed layer (reproduced with permission from [72] ©2011 Elsevier).

Thickness of the seed layer (nm)	Diameter of ZnO nanorods (nm)	Density of ZnO nanorods (μm^{-2})	Length of ZnO nanorods (nm)
20	30	213	1052
40	36	209	1007
160	51	184	998
320	72	169	967

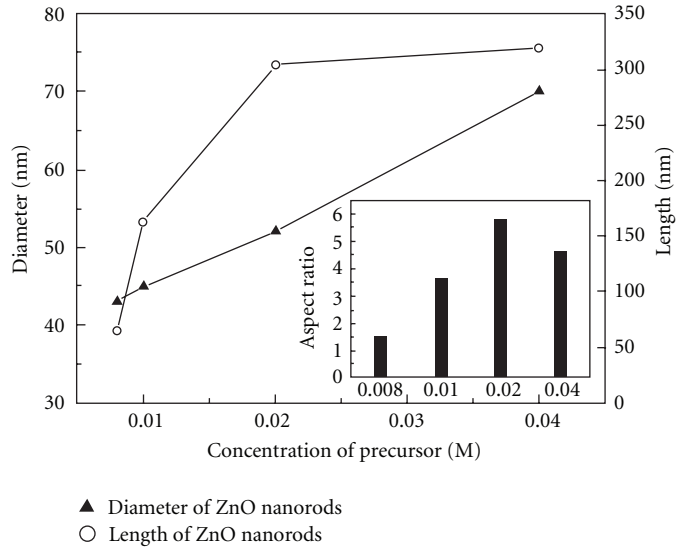

Figure 4: Average diameters, lengths, and aspect ratios of ZnO nanorods prepared from various precursor concentrations with a $Zn(NO_3)_2/C_6H_{12}N_4$ ratio of 5 (reproduced with permission from [83] ©2008 The American Ceramic Society).

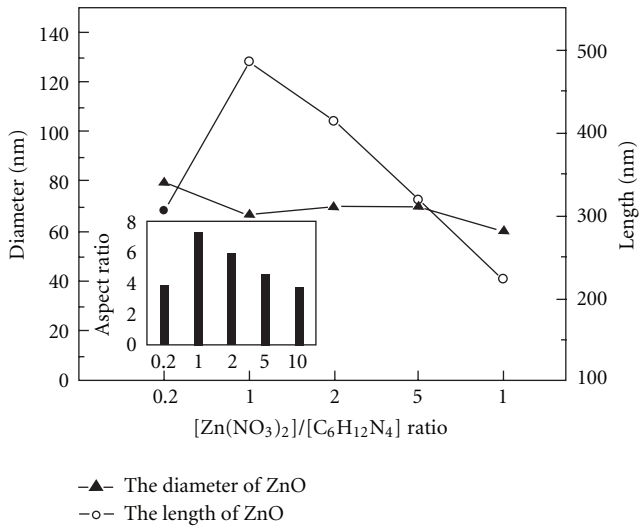

Figure 5: Average diameters, lengths, and aspect ratios of ZnO nanorods prepared in a 0.04 M precursor solution with various $Zn(NO_3)_2/C_6H_{12}N_4$ ratios (reproduced with permission from [83] ©2008 The American Ceramic Society).

unchanged after that. The authors explained that the growth rate is slowed down after this period due to depletion of the precursor. Baruah and Dutta [71] carried out ZnO nanowire experiments on zinc-acetate-seeded substrates for

Table 3: Average diameter of ZnO nanowires changes with growth time (data from [85]).

Growth time (hr)	Average diameter (nm)
0.5	35
1.0	37
1.5	55
2.0	90
2.5	100
3	100

different growth durations from 5 to 15 h. The SEM images showed that both length and diameter of the nanowires were increased with increasing growth duration time but the aspect ratio was reduced. Although nanowire growth slowed down after a certain period, the precursor supply for the ZnO nanowire growth can be replenished by repeatedly introducing fresh solution into the baths to keep up the growth rate [18, 86]. However, the diameter of the nanowires will also continue to increase and eventually connect together to form a ZnO film.

Effect of Initial Solution pH. Baruah and Dutta [45] studied the effect of pH variation on the dimension and morphology of ZnO nanorods grown by the hydrothermal synthesis

method. ZnO nanorods were grown on preseeded glass substrates using the same concentration of zinc nitrate and HTMA as the precursors. The pH of the reaction bath was found to change gradually from 6.4 to 7.3 in 5 h during the growth process. When the growth process was initiated in basic condition (pH 8–12), flower petal like ZnO nanostructures were obtained. Akhavan et al. [88] studied the effect of pH change from 7.5 to 11.44 on the growth of ZnO nanorods by using zinc nitrate and NaOH as precursors. They reported that the diameters of the nanowires are increased with increased pH until they formed a ZnO film when the pH reached a value of 11.44. For a precursor pH value of 11.33, fast growth of ZnO nanorods was observed on the seed layer. The fast growth of ZnO nanorods resulted in a reduction of the optical band gap energy due to the creation of greater number of defects in the nanorods during this fast growth.

Effect of Growth Substrate. One major advantage of the hydrothermal synthesis method is that almost any substrate can be used for the growth of vertical ZnO nanowires by using ZnO seeding layer. In this way, ZnO nanowires can grow on flat surface regardless of the substrate (polymer, glass, semiconductor, metal, and more) by only controlling the growth conditions. ZnO nanowires can also be grown on organic substrates. ZnO nanowires have been successfully grown on polydimethylsiloxane (PDMS) [89], polystyrene (PS) [90], polyethylene terephthalate (PET) [91], polyethylene fibers [92], microfibers [93], polyurethane [94], polyimide [95], paper [96], and other organic substrates like lotus leaf [97].

Effect of Growth Temperature. Sugunan et al. [68] carried out growth of ZnO nanowires at different temperatures by using equimolar zinc nitrate and HMTA from 60 to 95°C. They reported that hydrothermal growth carried out with 1 mM solution of the precursors at 95°C produced similar nanowire lengths as those grown at 65°C in the same growth period. Thus, the authors suggested that there is no significant difference in the nanowire growth process for different chemical bath temperatures.

Effect of Additives. The aspect ratio of ZnO nanowires could be affected by the addition of additives. Zhou et al. [98] reported the effect of the addition of polyethyleneimine (PEI) on ZnO nanorods and showed that the average diameter of the nanorods was reduced drastically from 300 nm to 40 nm as the PEI amount increased from 0 to 12% (v/v) in solution. The authors explained that the PEI molecules were adsorbed on the lateral facets of the ZnO nanorods due to the electrostatic affinity. Thus, the lateral growth of the nanorods could be largely limited. Chen et al. [99] studied the influence of PEI and NH_3 on the growth of ZnO nanowires. The SEM image showed that the diameter and length of ZnO nanowires decreased with the addition of PEI. With the addition of NH_3, the diameter of the ZnO nanowires was reduced even further.

Other Factors. Other factors affecting ZnO growth include the heating source, the Zn^{2+} source, the external electric field, and mechanical stirring. The use of microwave heating instead of conventional heating has recently received great interest [28, 100, 101]. The hydrolyzed method creates defective crystallites under microwave irradiation and leads to a faster growth process as compared to the conventional process [28, 102]. Zinc salts include acetates, nitrates, perchlorates, and chlorides. The counter ion of zinc often affects the crystallite morphology by acting as promoter or inhibitor in the nucleation and growth processes [80]. An external electric field could also affect the growth rate and depends on the electric field direction and the applied voltage. Mechanical stirring could increase the growth rate.

3.2.2. Other Solution Phase Synthesis Methods. Other solution phase synthesis methods include the microemulsion and ethanol base methods. Lim et al. [103] reported the preparation of ZnO nanorods by the microemulsion synthesis. The surfactant, such as ethyl benzene acid sodium salt (EBS), dodecyl benzene sulfonic acid sodium salt (DBS), and zinc acetate dispersed in xylene by stirring until a homogenous mixture, was obtained. Then the hydrazine and ethanol mixture solution was added drop by drop to the well-stirred mixture at room temperature. The resulting precursor-containing mixture was subsequently heated to 140°C and refluxed for 5 h. The resultant ZnO nanorods had an average diameter of 80 nm. In the microemulsion synthesis, the process is referred to as hydrothermal when it is carried out in an aqueous solution [104]. Wu et al. [105] synthesized ZnO nanorods by using a solvothermal base in an ethanol solution. The synthesis process consisted of a NaOH ethanol solution added drop by drop in a $Zn(NO_3)_2$ ethanol solution and the mixture transferred into a Teflon-lined stainless autoclave and heated at 160°C for 12 h.

3.3. Doping of ZnO Nanowires. Doping is the primary method of controlling semiconductor properties such as the band gap, electrical conductivity, and ferromagnetism. Many metals and nonmetals have been successfully used to dope ZnO nanowires by various synthesis methods. ZnO nanowire metal doping includes Ni [41], Co [106], Ga [107], Eu [108], Al [109], and Cu [110], and nonmetal doping includes C [111], N [112], P [113], and Cl [114]. Two different element codoped nanowires such as Mn + Co [115], Mn + Li [116], and Li + N [117], have also been studied by some research groups.

Li et al. [118] have reported doping of ZnO nanowires with Mn, Cr, and Co by a hydrothermal method from aqueous solutions of zinc nitrate hydrate, TM (TM=Mn, Cr, Co) nitrate hydrate, and HTMA. The experiments were carried out in vials and heated in an oven at 90°C for 3 h. Marzouki et al. [119] studied nitrogen-doped ZnO nanowires by using the MOCVD method. The precursors chosen were dimethylzinc-triethylamine (DMZn-TEN) for zinc, nitrous oxide (N_2O) for oxygen, and diallylamine for the nitrogen source. The MOCVD reactor operated at atmospheric pressure and 850°C. Das et al. [117] synthesized

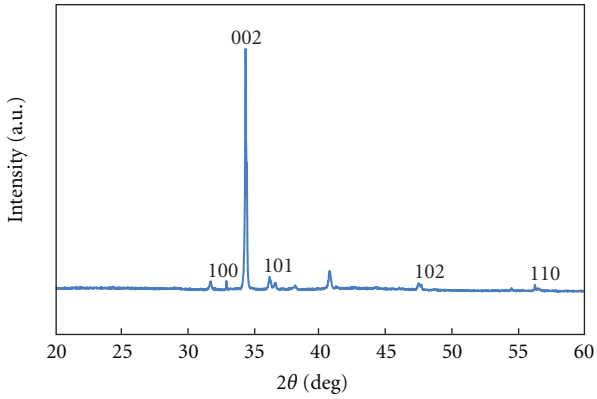

Figure 6: XRD of ZnO nanowires on a silicon substrate growth by the hydrothermal synthesis method (from [123] unpublished).

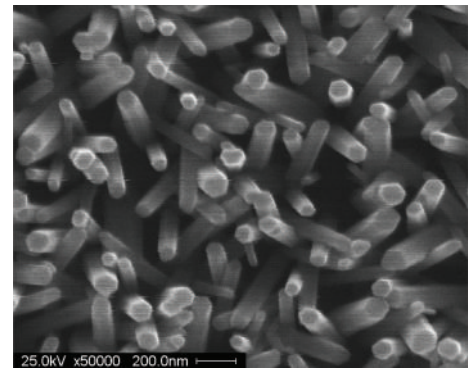

Figure 7: SEM image of the ZnO nanorods array on glass substrate by hydrothermal method (from [123] unpublished).

Li and N co-doped ZnO nanowires on a Si substrate by using the hydrothermal method. The process was carried out in three steps First, a thin ZnO seed layer (10 nm) was predeposited on Si by a sputtering technique. Second, Li-doped nanowires were synthesized by using $Zn(NO_3)_2$, HTMA, and LiCl for precursor growth at 80°C for 8 h in an oven. Finally, the nanowires were treated by rapid thermal annealing at 500°C in NH_3 environment for 30 min. It has been reported that Indium doping of ZnO nanowires cannot be carried out by hydrothermal synthesis due to formation of the $In(OH)_3$ phase [120]. Nevertheless, it could be realized by a postdeposition thermal annealing in an inert atmosphere [120] or by a vapor phase transport process [121].

4. Characterization/Properties

Under general conditions, ZnO is single crystalline and exhibits a hexagonal wurtzite structure. The structure of ZnO nanowires could be revealed by X-ray diffraction (XRD) and scanning electron microscopy (SEM). Figure 6 shows the XRD pattern of the ZnO nanowire growth on a silicon substrate by using the hydrothermal synthesis method. A dominant diffraction peak for (002) indicates a high degree of orientation with the *c*-axis vertical to the substrate surface. Figure 7 shows a top down image of ZnO nanowires [122]. Both XRD and SEM demonstrate the hexagonal wurtzite structure of the ZnO nanowires.

Further structural characterizations can be carried out by transmission electron microscopy (TEM) and high-resolution transmission electron microscopy (HRTEM). Figure 8(a) shows a low-resolution TEM image of ZnO nanowires with a homogeneous diameter size that does not vary significantly along the wire length. The HRTEM pattern measured for one individual nanowire is shown in Figure 8(b). The crystal lattice fringes spacing in the HRTEM image are 0.52 nm and fringes perpendicular to the wire axis is 0.26 nm. This measured plane spacing is characteristic of the (002) planes, showing the ZnO nanowire with a perfect lattice structure and verifing that the nanowires grow along the c-axis direction [124].

The ZnO nanowires obtained at different reaction times and examined by Raman spectra are presented in Figure 9. The peaks of the ZnO nanowires at 327, 378, 437, 537, and 1090 cm^{-1} were observed in all the samples. A narrow strong band at 437 cm^{-1} has been assigned to E_2 modes involving mainly a Zn motion corresponding to the band characteristic of the wurtzite phase. The band at 378 cm^{-1} (A_{1T} mode) indicates the presence of some degree of structural order-disorder in the ZnO lattice. The band bands at 327 cm^{-1} should be assigned to the second-order Raman spectrum. A band at 537 cm^{-1} is the contribution of the E_1 (LO) mode of ZnO associated with oxygen deficiency. The envelope of bands above 1090 cm^{-1} can be attributed to overtones and/or combination bands [125].

Figure 10 shows the UV-Visible absorption spectra of ZnO nanoparticles, ZnO nanowires, and ZnO/Fe nanowires. ZnO nanowires showed a larger enhancement absorption in the visible range as compared to ZnO nanoparticles. The ZnO/Fe nanowires exhibit even stronger absorption than the ZnO nanowires and nanoparticles in both the UV and the visible range implying that ZnO/Fe nanowires could more fully utilize most of the UV and visible light than the other two.

Figure 11 shows the FTIR spectrum of ZnO nanorods in the range of 2000–300 cm^{-1}. There is only one significant spectroscopic band around 417 cm^{-1} associated with the characteristic vibrational mode of Zn–O bonding [126].

The X-ray photoelectron spectroscopy (XPS) result Zn(2p) of the ZnO nanorods is shown in Figure 12. The peaks at 1021.4 and 1044.6 eV in the spectrum corresponding to the doublet of Zn ($2p_{3/2}$) and ($2p_{1/2}$), respectively, can be attributed to the formation of hexagonal ZnO nanorods [9].

Figure 13 shows the photopotential response of a ZnO nanowire electrode under UV irradiation. When the UV light is switched on, electron-hole pairs are generated and produce a photocurrent. The UV irradiation changes the current abruptly with some variation, and the photo-potential is sharply reduced when the light is switched off [35].

In addition to the above characterizations, ZnO nanowires also exhibit many other unique chemical and physical properties for many applications such as large surface areas, piezoelectric, piezotronic, and optical.

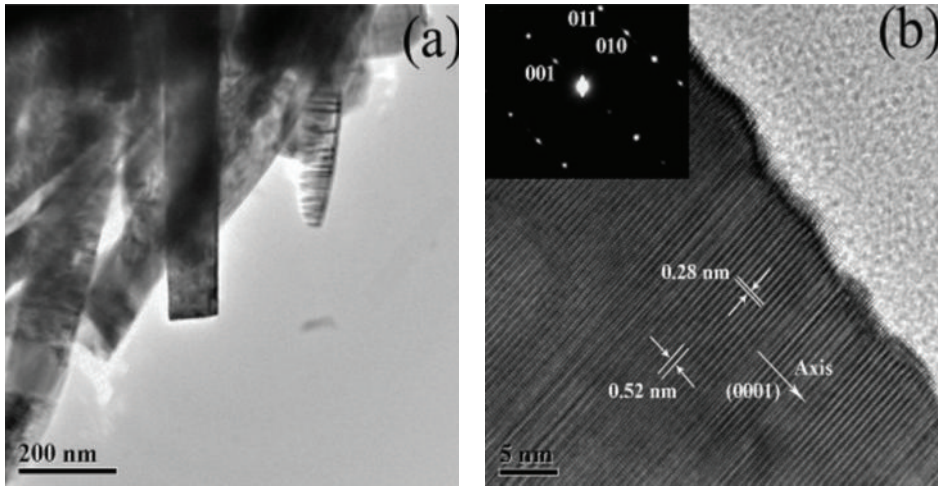

Figure 8: (a) TEM of ZnO nanowires on an ITO substrate showing a general view. (b) HRTEM image showing individual nanowires with [0 0 2] growth direction. Inset shows selected electron diffraction (SAED) patterns (reproduced with permission from [124] ©2010, Elsevier).

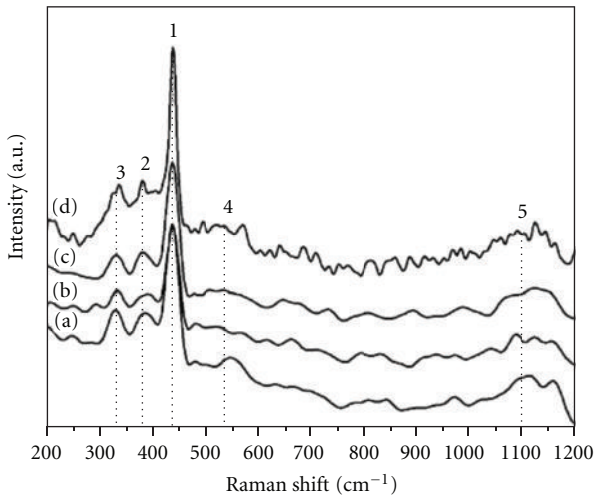

Figure 9: Raman spectra of the ZnO structures obtained by the hydrothermal method at 130°C for (a) 30 min, (b) 60 min, (c) 120 min, and (d) 180 min (reproduced with permission from [125] ©2010 Elsevier).

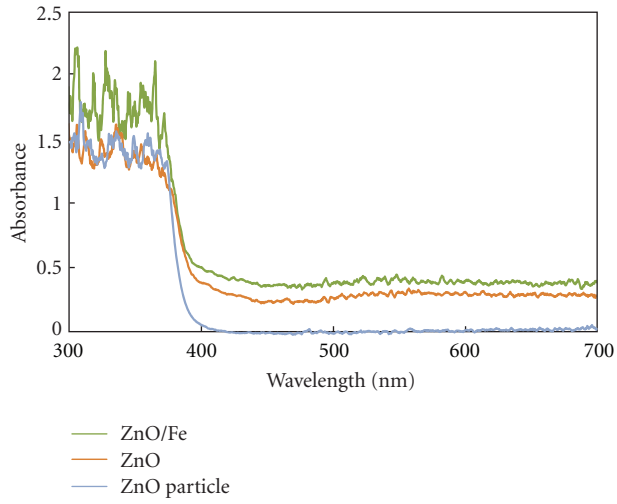

Figure 10: UV-Visible absorption spectra of ZnO nanoparticle, ZnO and ZnO/Fe nanowires (from [123] unpublished).

5. Applications

ZnO nanowires can be used for a number of applications in different fields due to the unique electrical, optical, and mechanical properties.

5.1. Sensor

5.1.1. Gas Sensor. ZnO is one of the earliest discovered and most widely used oxide gas sensing materials. ZnO functions as a gas sensitive material due to its electrical conductivity that can be dramatically affected by the adsorption or desorption of gas molecules on its surface [127]. 1D nanostructured devices such as nanowires are more sensitive and selective due to their high aspect ratio giving rise to

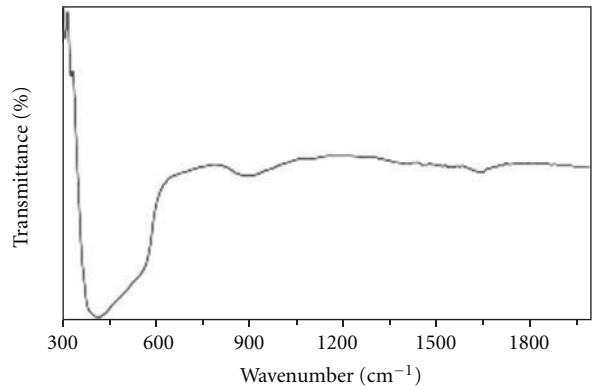

Figure 11: FTIR spectrum of ZnO nanorods prepared at 200°C for 20 h using NaOH (reproduced with permission from [126] ©2010 Elsevier).

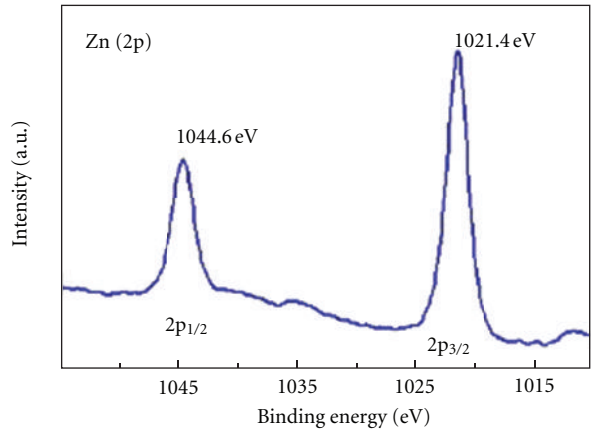

Figure 12: Zn(2p)XPS spectrum of synthesized ZnO nanorods on a ZnO thin film (reproduced with permission from [9] ©2011 Elsevier).

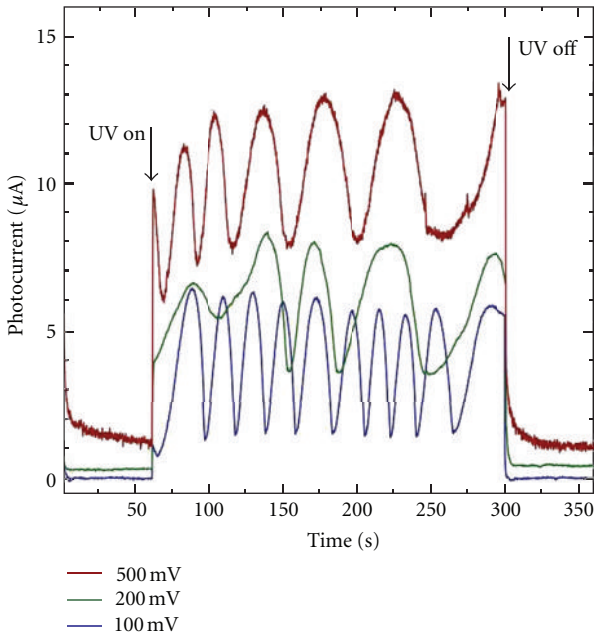

Figure 13: Photocurrent response to UV light at different DC biases (reproduced with permission from [35] ©2011 American Chemical Society).

a large surface area. There are many gasses that can be detected by ZnO nanowires, such as NO [128], NO_2 [129], CO [130], NH_3 [127], H_2 [131], O_2 [132], and ethanol [133]. A resistor type NO_2 gas sensor based on the ZnO nanorod was reported by Oh et al. [134] using a sonochemical route. The vertically aligned ZnO nanorods were grown on a Pt-electrode patterned alumina substrate under ambient conditions. The ZnO nanorod gas sensor was highly sensitive to the NO_2 gas with a very low detection limit of 10 ppb at 250°C and short response and recovery time (Figure 14). Wei et al. [135] reported a room temperature NH_3 gas sensor based on a ZnO nanorod array produced by hydrothermal decomposition on an Au electrode. Recently, Oh and Jeong [136] fabricated CO sensors based on aligned ZnO nanorods

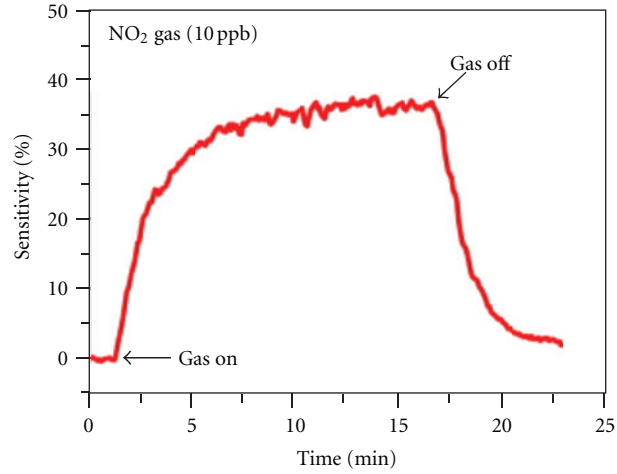

Figure 14: Response curve of a ZnO gas sensor exposed to 10 ppb NO_2 gas at 250°C (reproduced with permission from [134] ©2009 Elsevier).

on a substrate and exhibited high sensitivity to CO gas with the low detection limit of 1 ppm at 350°C.

5.1.2. Biosensor. Recently, ZnO nanostructures have attracted interest in biosensor applications due to many advantages, including nontoxicity, biosafety, bio-compatibility, high electron-transfer rates, and combination with immobilized enzymes [137]. The high isoelectric point (IEP) of ZnO (IEP 9.5) makes it a good matrix for immobilizing low IEP acidic proteins or DNA by electrostatic interactions with high binding stability [138]. In addition, ZnO has high ionic bonding (60%), and it dissolves very slowly at normal biological pH environments. Liu et al. [139] have constructed an ampere-metric glucose biosensor based on aligned ZnO nanorod films formed directly on the surface of ITO glass. The biosensor exhibited a linear response to glucose from 5 μM to 300 μM and a limit of detection of 3 μM (Figure 15(a)). The biosensor also showed good selectivity for glucose. In an air-saturated and stirred 0.01 M PBS containing 5 μM glucose, there was no significant change of the ampere-metric response by the injection of 10 μM UA and AA, respectively (Figure 15(b)). Ibupoto et al. [140] have demonstrated the fabrication of a ZnO-nanorod-based biosensor with good reproducibility and selectivity for the quick monitoring of penicillin with the immobilization of the penicillinase enzyme by the simple physical adsorption method. The authors showed that the potentiometric response of the sensor configuration revealed good linearity over a large concentration range from 100 μM to 100 mM. Choi et al. [141] described a ZnO nanowire field-effect-transistor- (FET-) based biosensor for the detection of low level biomolecular interactions. The ZnO nanowire biosensor could detect as low as 2.5 nM of the streptavidin with a current increase of 7.5 nA.

5.2. UV Detector. UV detection is another promising optical application of ZnO nanowires [142–144]. The UV detector

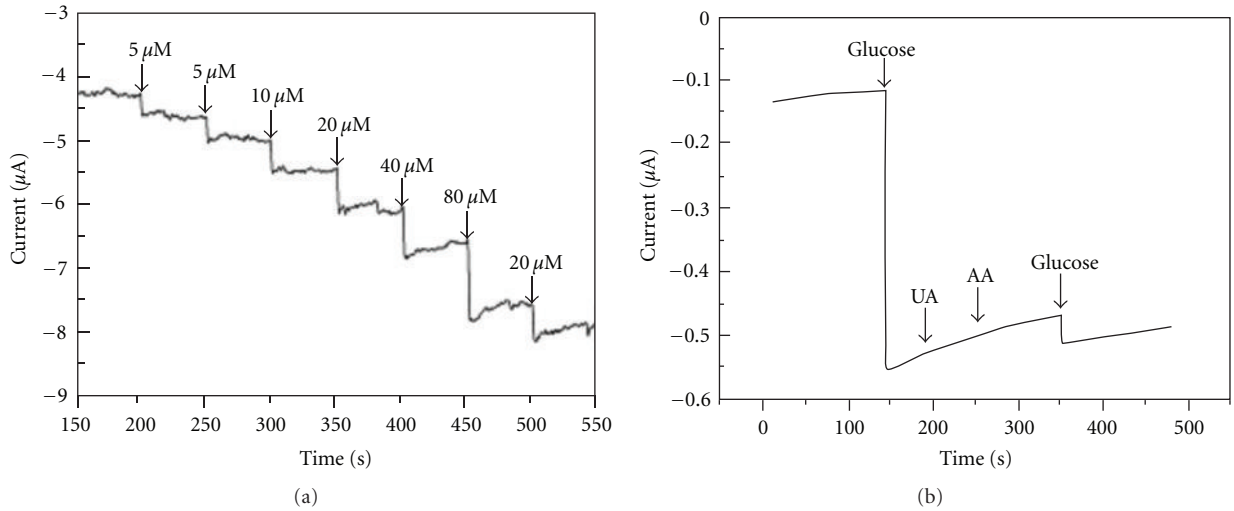

Figure 15: (a) Typical steady-state response of the biosensor by the successive addition of specific concentrations of glucose to air-saturated and stirred 0.01 M pH 7.4 PBS solution at −100 mV. (b) Effect of interfering species on the biosensor response (reproduced with permission from [139] ©2009 Elsevier).

utilizes the electric potential of the ZnO nanowires changed under UV irradiation. Chen et al. [143] constructed a UV photodetector by contacting a circular spiral structure ZnO nanowire with 30 nm IrO_2 electrodes. The *I-V* measurement showed that the curve corresponded to the Schottky metal-semiconductor contacts with the photo-generated current reaching 5.11×10^{-7} A, under a bias voltage of 5 V, and the photocurrent being 2 orders of magnitude larger than the dark current (Figure 16). Li et al. [145] proposed a method of fabricating a ZnO bridging nanowire structure exhibiting nanowatt UV detection. The electrodes were formed by the thick ZnO layers covering the Au-catalyst-patterned areas on the substrate, and the sensing elements consisted of the ultralong ZnO nanowires bridging the electrodes. The device exhibited drastic changes (10–10^5 times) in current under a wide range of UV irradiance (10^{-8}–10^{-2} W cm^{-2}). Moreover, the detector showed fast response (rise and decay times of the order of 1 s) to UV illumination in air. Yang et al. [146] synthesized a simple self-assembled lateral growth ZnO nanowire photodetector with the photocurrent of the ZnO nanowires under UV illumination being twice as larger as the dark current with a bias voltage of 5 V. Lin et al. [147] reported that loading of Ag particles in ZnO nanowires produces an enhanced photoresponse. Chang et al. [148] combined the ZnO nanorods with graphene enabling the UV sensor to reach 22.7 A/W.

5.3. UV Laser. Room temperature of ZnO-nanowire-based UV lasing has been recently demonstrated [149]. Figure 17 shows a typical room temperature photoluminescence (PL) spectrum of ZnO nanorods with an excitation wavelength of 325 nm at room temperature [150]. The spectrum exhibits two bands including a strong ultraviolet emission at 378 nm (or 3.28 eV) and a weak spectral band in the visible region. The UV emission was contributed to the near band edge emission of the wide band gap of ZnO. Visible emission is due to the presence of various point defects such as oxygen vacancies.

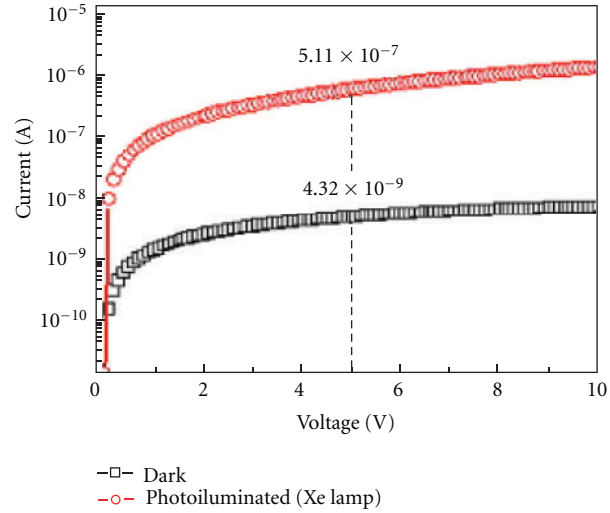

Figure 16: *I-V* characteristics of a ZnO photodetector in the dark and under Xe illumination (reproduced with permission from [143] ©2009 Elsevier).

5.4. Light-Emitting Diode. The output power of GaN LEDs with ZnO nanotip arrays can be enhanced by up to 50% times [151]. A heterojunction LED could be fabricated by the growth of vertically aligned ZnO nanowires on a p-GaN substrate and employed indium tin oxide (ITO)/glass to combine and package [152, 153]. Figure 18 shows the electroluminescence (EL) spectra of ZnO NWs/p-GaN/ZnO nanowire heterostructure at a DC current of 20 mA. A UV-blue electroluminescence (EL) emission was observed from the nanowire-film heterojunction diodes. Most of the

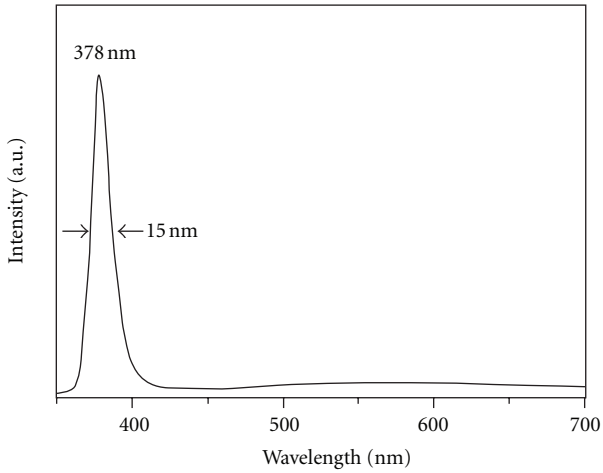

Figure 17: Room temperature PL spectra of ZnO nanorods (λ_{exc} = 325 nm) (reproduced with permission from [150] ©2009 Elsevier).

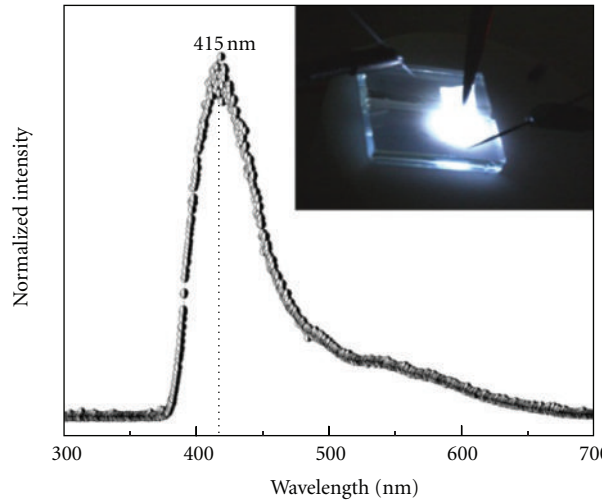

Figure 18: EL spectra of ZnO nanowires/p-GaN/ZnO nanowires heterostructure at a DC current of 20 mA. The inset is a photograph of the emission of blue light by the heterojunction LED under dc bias (reproduced with permission from [152] ©2009 American Institute of Physics).

currently developed ZnO LEDs are based on heterojunctions. However, a ZnO rod *p*-*n* homojunction LED with an ion-implanted P-doped *p*-type ZnO could also be fabricated [154].

5.5. Dye-Sensitized Solar Cells. Dye-sensitized solar cells (DSSCs), which are based on oxide semiconductors and organic dyes or metal organic complex dyes, are one of the most promising candidate systems to achieve efficient solar-energy because they are flexible, inexpensive, and easier to manufacture than silicon solar cells [155]. ZnO-based DSSC technology alternative to TiO_2 is considered as one of the most promising materials for solar cells due to a faster electron transport with reduced recombination loss and its ease of crystallization and anisotropic growth. Ko et al. [87] compared different fabricated ZnO nanowire DSSCs that included lengthwise growth (LG) and branched growth (BG). They showed that the overall light-conversion efficiency of the branched ZnO nanowire DSSCs was much higher than the upstanding ZnO nanowires (Figure 19 and Table 4). The reason for the improvement is the enhanced surface area for higher dye loading and light harvesting and the reduction of charge recombination by providing direct conduction pathways along the crystalline ZnO "nanotree" multigeneration branches.

Lupan et al. [124] studied the well-aligned arrays of vertically oriented ZnO nanowires electrodeposited on ITO-coated glass for dye-sensitized solar cells. The maximum overall photovoltaic conversion efficiency was 0.66% at 100 mW/cm^2. Cheng et al. [156] fabricated branched ZnO nanowires on conductive glass substrates via a solvothermal method for dye-sensitized solar cells. The short-circuit current density and the energy conversion efficiency of the branched ZnO nanowire DSSCs are 4.27 mA/cm^2 and 1.51%, which are higher than those pf the bare ZnO nanowire. Sudhagar et al. [13] reported jacks-like ZnO nanorod architecture as a photoanode in dye-sensitized solar cells and the result exhibited a higher conversion efficiency of η = 1.82% (V_{oc} = 0.59 V, J_{sc} = 5.52 mA cm^{-2}) than that of the branch-free ZnO nanorods electrodes (η = 1.08%, V_{oc} = 0.49 V, J_{sc} = 4.02 mA cm^{-2}).

5.6. Nanogenerator. Due to the noncentrosymmetric symmetry of the wurtzite structure, ZnO exhibits a strong piezoelectric behavior. Recently, nanogenerators (NGs) have been developed by utilizing the piezoelectric effect of ZnO nanowires for scavenging tiny and irregular mechanical energy such as air flow vibrations and body movements [159–162]. Zhu et al. [157] reported a flexible high output nanogenerator (HONG), based on a lateral ZnO nanowire array for harvesting mechanical energy, for driving a small commercial electronic component. The electrical output of a single layer of the HONG structure reached a peak voltage of 2.03 V and a current of 107 nA with a peak power density of 11 mW/cm^3 (Figure 20). The energy generation efficiency was 4.6%. The generated electric energy was successfully used to light up a commercial light-emitting diode (LED). The authors also predicted that the peak output power density of 0.44 mW/cm^2 and a volume density of 1.1 W/cm^3 could be realized by optimizing the density of the nanowires on the substrate and using multilayer integration.

Hu et al. [163] integrated a nanogenerator onto a tire inner surface and scavenged mechanical energy from the deformation of the tire during its motion. The nanogenerator directly powers a liquid crystal display (LCD) screen. Xu and Wang [164] designed a compact hybrid cell based on the combination of a piezoelectric nanogenerator and a DSSC in one compact structure. The compact hybrid cell showed a significant increase in output power. Cha et al. [165] fabricated a sound-driven piezoelectric ZnO nanowire-based nanogenerator and obtained an AC output voltage of about 50 mV.

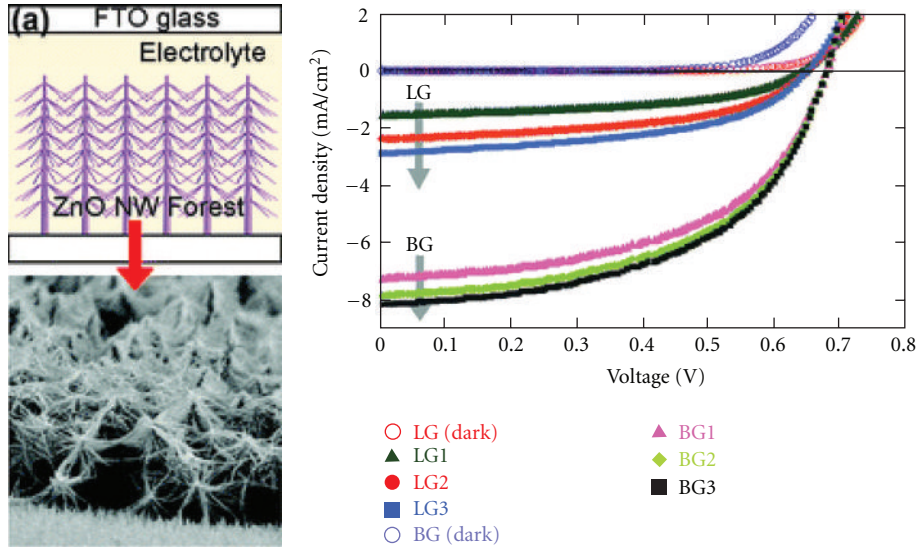

(a) (b)

Figure 19: (a) Schematic structure of a solar cell and (b) *J-V* curve of dye-sensitized solar cells with different fabricated ZnO nanowires (reproduced with permission from [87] ©2011 American Chemical Society).

Table 4: Characteristics and parameters of the "Nanoforest" DSSC Solar Cells shown in Figure 19 (reproduced with permission from [87] ©2011 American Chemical Society).

Symbol	Backbone NW length [μm]	Branching times	Configuration	Efficiency [%]	J_{sc} [mA/cm^2]	V_{oc} [V]	FF
LG1	7	0		0.45	1.52	0.636	0.480
LG2	13			0.71	2.37	0.64	0.486
LG3	18			0.85	2.87	0.645	0.484
BG1	7	1		2.22	7.43	o.681	0.522
BG2	13			2.51	8.44	0.683	0.531
BG3		2		2.63	8.78	0.680	0.530

5.7. Field Emission Devices. ZnO nanowires are considered as candidates of field emitters due to their high melting point and high stability under an oxygen environment as compared to CNTs [166, 167]. Hwang et al. [166] reported vertical ZnO nanowires grown on grapheme/PDMS substrates for transparent and flexible field emission. The ZnO nanowires/graphene hybrids showed excellent field emission properties with the low turn-on field values of 2.0 V μm^{-1}, 2.4 V μm^{-1}, and 2.8 V μm^{-1} measured for convex, flat, and concave deformations, respectively. Kang et al. [168] presented ZnO nanowire patterned growth for the field emission device. The optimum patterned ZnO nanowire field emission device fabricated with the current approach was found to exhibit a low turn-on electric field value (1.60 μm V^{-1}) due to the decrease in the field emission screening effect that results from the radial structures of the micropatterned ZnO nanowires arrays. Chen et al. [169] synthesized ZnO nanowires on a ZnO:Ga/glass substrate. UV illumination increased the ZnO nanowire field emission and reduced the turn-on electric field from 5.1 to 2.1 V/μm at a current density of 1 μA/cm^2. Doping by certain metals for enhancement of the field emission device performance has also been reported such as Sn [170] and Ga [171].

5.8. Field Effect Transistor. A typical nanowires field effect transistor (FET) consists of a semiconductor nanowire

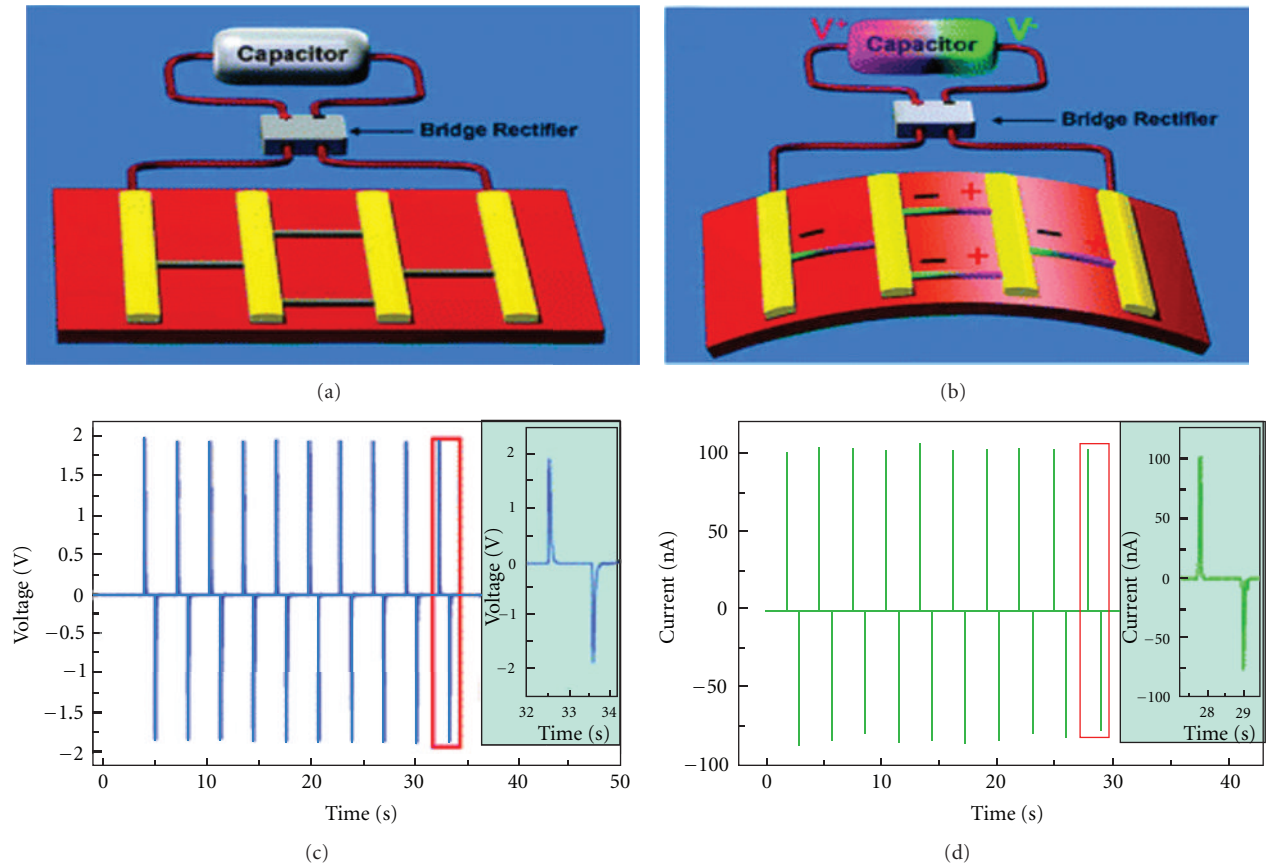

Figure 20: Working principle and output measurement of the HONG. (a) Schematic diagram of the HONG structure without mechanical deformation, in which gold is used to form Schottky contacts with the ZnO nanowire arrays. (b) Demonstration of the output scaling-up when mechanical deformation is induced, where the "±" signs indicate the polarity of the local piezoelectric potential created in the nanowires. (c) Open circuit voltage measurement of the HONG. (d) Short circuit current measurement of the HONG. The measurement is performed at a strain of 0.1% and strain rate of 5% s^{-1} with a deformation frequency of 0.33 Hz. The insets are the enlarged view of the boxed area for one cycle of deformation (reproduced with permission from [157] ©2010 American Chemical Society).

(ZnO, etc.) connected with two electrodes at two ends and placed on a flat substrate that serves as a gate electrode. The current flow from the drain to the source along the nanowire is controlled by the applied gate voltage or the chemical/biochemical species adsorbed on the surface of the nanowires. Recently, piezoelectric-FET (PE-FET) has been demonstrated by coupling the semiconductive and piezoelectric properties of ZnO, which is defined as the piezotronics effect [172–174]. The working principle of PE-FET relies on the piezoelectric potential of the nanowire under straining and serves as the gate voltage for controlling the current flow from the drain to source [175].

5.9. Photocatalysis. ZnO nanowires used as photocatalysts have been recently reported by many research groups [158, 176–178]. Sugunan et al. [158] described a continuous flow water purification system by the fabrication of ZnO nanowires grown on flexible poly-L-lactide nanofibers. The continuous flow photocatalytic decomposition of organic compounds in water has no need for separation of the photochemically active material from the reservoir, and the purified water can be directly collected from the reservoir (Figure 21). The various organic pollutants that have been tested and removed under UV light illumination include methylene blue, monocrotophos, and diphenylamine. The results demonstrated that simultaneous photocatalytic decomposition of more than one organic contaminant is possible by using the polymer-ZnO nanostructure. The authors also stated that the fabrication can be easily scaled up and the whole photocatalytic water treatment setup can easily be adapted either as a point-of-use system or centralized large-scale water purification system. Baruah et al. [92] reported the growth of ZnO nanowires on woven polyethylene fibers for photocatalytic applications. Photocatalytic activity testing was carried out in UV light and degraded 0.01 mM of methylene blue. The results revealed that ZnO nanowires grown on polyethylene fibers accelerate the photocatalytic degradation process by a factor of 3 as compared to just polyethylene fibers. Kuo et al. [179] synthesized ultralong ZnO nanowires on silicon substrates by the vapor transport process and used them as recyclable photocatalysts for the degradation of rhodamine B and 4-chlorophenol. The results showed only a slight decrease in the photodecomposition rate after 10 cycles. SEM images indicated that the nanowire appearance and

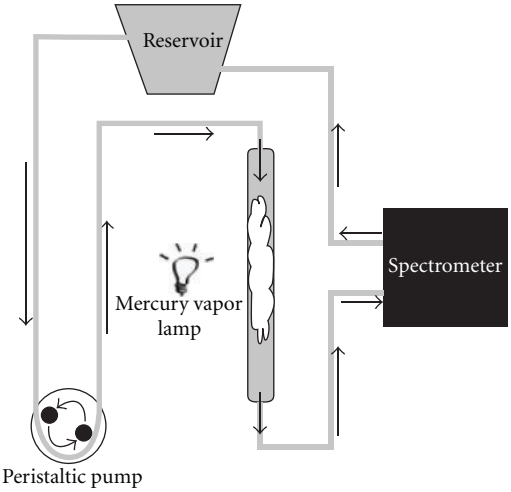

Figure 21: Schematic of a continuous-flow photocatalytic water treatment system (reproduced with permission from [158] ©2010 The American Ceramic Society).

density did not show noticeable change after 10 experiment cycles. Baruah et al. [96] synthesized ZnO nanorods on a paper substrate as photocatalytic paper. The photocatalytic activity was carried out by the degradation of methylene blue and methyl orange under 963 W/m^2 visible light and inactivity of *Escherichia coli* under 11 W/m^2 visible light. The results showed that the photocatalytic paper could degrade organic dye and also inhibit the growth of *Escherichia coli* under room light conditions (11 W/m^2). Sapkota et al. [18] investigated the inactivation of microbes in water by the visible light photocatalysis of ZnO nanorods. ZnO nanorods were grown on a glass substrate by the hydrothermal route and employed in the inactivation of *Escherichia coli* and *Bacillus subtilis* in water. The cell membrane damage and DNA degradation were observed under the visible light photocatalytic process. Wang et al. [19] also studied the photocatalytic degradation of *Escherichia coli* membrane cell in the presence of ZnO nanowires. The SEM images showed that the outer membrane of *Escherichia coli* was destroyed completely in the presence of ZnO nanowires under UV irradiation and the cells became twisted shapes without a mechanically strong network.

Surface properties such as surface defects and oxygen vacancies of photocatalysts play a significant role in the photocatalytic activity. ZnO nanowire crystalline defects exist primarily due to oxygen vacancies [28]. Nanoparticles with crystalline defects are capable of exhibiting visible light photocatalysis even without doping with transition metals [67]. Baruah et al. [28] reported a fast crystallization ZnO nanorods synthesis method to increase the surface defect of the ZnO nanowires. Compared to the conventional hydrothermal synthesis method, an increase in the density of vacancies and surface defects in the nanorod crystals were obtained through accelerated crystallization using microwave hydrothermal and subsequent fast quenching reactions. The authors also compared the photocatalytic activity of conventional and microwave-grown nanorods in the degradation of methylene blue. The photocatalysis was carried out under 72 klx of visible light. The microwave hydrolyzed nanorods showed better photocatalytic activity as compared to the conventional synthesized nanorods. The authors also stated that ZnO nanorods grown through fast crystallization under microwave irradiation not only created defective crystallites for better photocatalysis but also saved time and energy during the growth process due to faster synthesis. Zhang and Zhu [101] reported that ZnO nanostructures have enhanced photocatalytic activity by using the microwave-assisted solvothermal synthesis method. Zhu et al. [180] studied the microwave-assisted hydrothermal synthesis of ZnO nanorod-assembled microspheres for photocatalysis and demonstrated that the as-prepared ZnO had excellent optical properties and higher photocatalytic activity due to surface defects.

To further increase the photoactivity of ZnO nanowires, our group has synthesized ZnO/Fe nanowires by the growth of ZnO nanowires on the Fe-doped ZnO seeding layer using the hydrothermal method. The photocatalytic activity was evaluated by photodegradation of dichlorobenzene (DCB) and methyl orange (MO) in water. The experiments were carried out under white light (60 W/m^2 in visible plus 2 W/m^2 in UV) or UV light (30 W/m^2) irradiation. The results showed that the ZnO/Fe nanowires exhibited enhanced photocatalytic activity as compared with pure ZnO nanowires under different light irradiation as well as different contaminants. For the decontamination of DCB (Figures 22(a) and 22(b)), ZnO/Fe nanowires exhibited greater photoactivity than pure ZnO nanowires under white light as well as UV light irradiation. When compared to TiO_2 (P25), ZnO/Fe nanowires show better photoactivity than P25 under white light irradiation. For the decontamination of MO (Figures 22(c) and 22(d)), ZnO/Fe nanowires also exhibit an enhanced photocatalytic activity as compared with pure ZnO nanowires under white light as well as UV light irradiation. The results demonstrate that ZnO/Fe nanowires could be a better photocatalyst in sunlight.

Doping transition metal ions is a strategy for improving the visible light photocatalytic activity, by lowering the band gap, resulting from the creation of dopant energy levels below the conduction band [181]. Wu et al. [182] synthesized 3% Cr-doped ZnO nanowires and showed that Cr-doped ZnO nanowires have better photoactivity for decoloration of methyl orange as compared to pure ZnO and P25 under visible light irradiation. Lu et al. [183] reported cobalt-doped ZnO nanorods as photocatalyst, and revealed that the Co-doped ZnO samples have an extended light absorption range and increased photocatalytic activity of alizarin red dye decomposition under visible light irradiation as compared with pure ZnO nanorods. Jia et al. [184] studied the photocatalytic activity of La-doped ZnO nanowires. The results showed an increase in the photocatalytic activity of La-doped ZnO nanowires in the degradation of Rhodamine B (RhB) with the optimal doping content being about 2% in terms of photocatalytic activity efficiency. Wu et al. [185] reported that the photocatalytic activity of 3% Sb-doped ZnO nanowires is superior to that of undoped ZnO nanowires under both UV and visible-light testing. Mahmood et al. [186] reported enhanced visible light

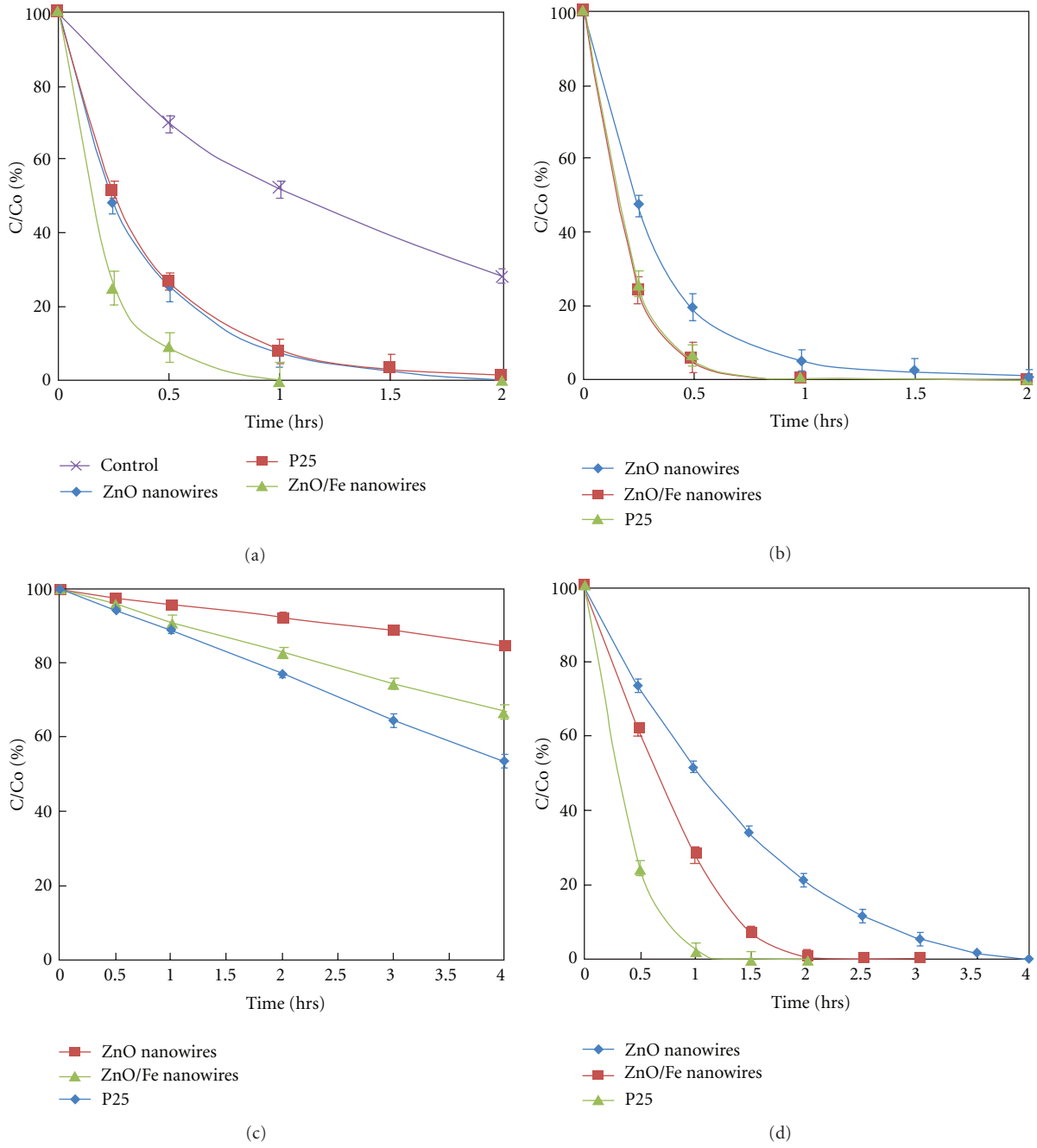

Figure 22: Photocatalyst activity testing: (a) degradation of DCB under white light irradiation; (b) degradation of DCB under UV light irradiation; (c) photodegradation of MO in visible light irradiation; (d) photodegradation of MO in UV light irradiation. The control of DCB is also reduced due to the volatility of the DCB (from [123] unpublished).

photocatalysis by manganese doping or rapid crystallization with ZnO nanoparticles. Li et al. [187] investigated the structural, electronic, and optical properties of Ag-doped ZnO nanowires using first-principles calculations based on DFT. The results provide theoretical evidence that Ag-doped ZnO nanowires could also have potential applications in photocatalysis due to the increase in visible-photocatalytic activity. Other dopings of ZnO nanowires, such as Sn [105] and Na [188], have also been reported and have shown an enhancement of photocatalytic activity for the degradation of organic compounds in water. In addition to doping, Jung and Yong [189] reported the fabrication of CuO–ZnO nanowires on a stainless steel mesh for highly efficient photocatalytic applications.

6. Conclusions

This paper provides an overview of the synthesis, characterization, and applications of ZnO nanowires. The hydrothermal synthesis method is simple and efficient and it has

received increased attention. A mixture of zinc nitrate and hexamine as precursor is the most popular. Due to the unique properties of the material, ZnO nanowires are attractive for a number of potential applications such as photocatalysis, solar cells, sensors, and generators. Among the applications of ZnO nanowires, photocatalysis is being increasingly used for environmental protection. Further research is needed to improve the quality of ZnO nanowires and large-scale produce ZnO nanowires for practical industrial applications. Based on this paper, ZnO nanowires promise to be one of the most important materials in photocatalytic as well as others applications.

Acknowledgment

The research leading to this paper was funded by the State of Florida through the Florida Energy Systems Consortium (FESC) funds.

References

[1] W. Liu, A. B. Greytak, J. Lee et al., "Compact biocompatible quantum dots via RAFT-mediated synthesis of imidazole-based random copolymer ligand," *Journal of the American Chemical Society*, vol. 132, no. 2, pp. 472–483, 2010.

[2] A. Hoshino, K. Fujioka, T. Oku et al., "Quantum dots targeted to the assigned organelle in living cells," *Microbiology and Immunology*, vol. 48, no. 12, pp. 985–994, 2004.

[3] B. Weintraub, Z. Zhou, Y. Li, and Y. Deng, "Solution synthesis of one-dimensional ZnO nanomaterials and their applications," *Nanoscale*, vol. 2, no. 9, pp. 1573–1587, 2010.

[4] Y. Xia, P. Yang, Y. Sun et al., "One-dimensional nanostructures: synthesis, characterization, and applications," *Advanced Materials*, vol. 15, no. 5, pp. 353–389, 2003.

[5] G. C. Yi, C. Wang, and W. I. Park, "ZnO nanorods: synthesis, characterization and applications," *Semiconductor Science and Technology*, vol. 20, pp. S22–S34, 2005.

[6] Z. L. Wang, "Ten years' venturing in ZnO nanostructures: from discovery to scientific understanding and to technology applications," *Chinese Science Bulletin*, vol. 54, no. 22, pp. 4021–4034, 2009.

[7] F. Lu, W. Cai, and Y. Zhang, "ZnO hierarchical micro/nanoarchitectures: solvothermal synthesis and structurally enhanced photocatalytic performance," *Advanced Functional Materials*, vol. 18, no. 7, pp. 1047–1056, 2008.

[8] J. Zhou, N. Xu, and Z. L. Wang, "Dissolving behavior and stability of ZnO wires in biofluids: a study on biodegradability and biocompatibility of ZnO nanostructures," *Advanced Materials*, vol. 18, no. 18, pp. 2432–2435, 2006.

[9] M. Mehrabian, R. Azimirad, K. Mirabbaszadeh, H. Afarideh, and M. Davoudian, "UV detecting properties of hydrothermal synthesized ZnO nanorods," *Physica E*, vol. 43, no. 6, pp. 1141–1145, 2011.

[10] C. F. Klingshirn, "ZnO: material, physics and applications," *ChemPhysChem*, vol. 8, no. 6, pp. 782–803, 2007.

[11] S. Chu, G. Wang, W. Zhou et al., "Electrically pumped waveguide lasing from ZnO nanowires," *Nature Nanotechnology*, vol. 6, no. 8, pp. 506–510, 2011.

[12] J. H. Na, M. Kitamura, M. Arita, and Y. Arakawa, "Hybrid p-n junction light-emitting diodes based on sputtered ZnO and organic semiconductors," *Applied Physics Letters*, vol. 95, no. 25, Article ID 253303, 2009.

[13] P. Sudhagar, R. S. Kumar, J. H. Jung et al., "Facile synthesis of highly branched jacks-like ZnO nanorods and their applications in dye-sensitized solar cells," *Materials Research Bulletin*, vol. 46, no. 9, pp. 1473–1479, 2011.

[14] Z. L. Wang, R. Yang, J. Zhou et al., "Lateral nanowire/nanobelt based nanogenerators, piezotronics and piezo-phototronics," *Materials Science and Engineering R*, vol. 70, no. 3–6, pp. 320–329, 2010.

[15] J. Xu, J. Han, Y. Zhang, Y. Sun, and B. Xie, "Studies on alcohol sensing mechanism of ZnO based gas sensors," *Sensors and Actuators, B*, vol. 132, no. 1, pp. 334–339, 2008.

[16] C. Y. Lu, S. J. Chang, S. P. Chang et al., "Ultraviolet photodetectors with ZnO nanowires prepared on ZnO:Ga/glass templates," *Applied Physics Letters*, vol. 89, no. 15, Article ID 153101, 2006.

[17] S. Cho, S. Kim, J. W. Jang et al., "Large-scale fabrication of sub-20-nm-diameter ZnO nanorod arrays at room temperature and their photocatalytic activity," *Journal of Physical Chemistry C*, vol. 113, no. 24, pp. 10452–10458, 2009.

[18] A. Sapkota, A. J. Anceno, S. Baruah, O. V. Shipin, and J. Dutta, "Zinc oxide nanorod mediated visible light photoinactivation of model microbes in water," *Nanotechnology*, vol. 22, no. 21, Article ID 215703, 2011.

[19] X. Wang, W. Wang, P. Liu, P. Wang, and L. Zhang, "Photocatalytic degradation of E.coli membrane cell in the presence of ZnO nanowires," *Journal Wuhan University of Technology, Materials Science Edition*, vol. 26, no. 2, pp. 222–225, 2011.

[20] S. S. Srinivasan, J. Wade, E. K. Stefanakos, and Y. Goswami, "Synergistic effects of sulfation and co-doping on the visible light photocatalysis of TiO_2," *Journal of Alloys and Compounds*, vol. 424, no. 1-2, pp. 322–326, 2006.

[21] H. Zhang, X. Lv, Y. Li, Y. Wang, and J. Li, "P25-graphene composite as a high performance photocatalyst," *ACS Nano*, vol. 4, no. 1, pp. 380–386, 2010.

[22] D. Y. Goswami, "Decontamination of ventilation systems using photocatalytic air cleaning technology," *Journal of Solar Energy Engineering, Transactions of the ASME*, vol. 125, no. 3, pp. 359–365, 2003.

[23] A. Vohra, D. Y. Goswami, D. A. Deshpande, and S. S. Block, "Enhanced photocatalytic inactivation of bacterial spores on surfaces in air," *Journal of Industrial Microbiology and Biotechnology*, vol. 32, no. 8, pp. 364–370, 2005.

[24] N. Kislov, J. Lahiri, H. Verma, D. Y. Goswami, E. Stefanakos, and M. Batzill, "Photocatalytic degradation of methyl orange over single crystalline ZnO: orientation dependence of photoactivity and photostability of ZnO," *Langmuir*, vol. 25, no. 5, pp. 3310–3315, 2009.

[25] S. Srinivasan, D. Escobar, Y. Goswami, and E. Stefanakos, "Effects of catalysts doping on the thermal decomposition behavior of $Zn(BH_4)_2$," *International Journal of Hydrogen Energy*, vol. 33, no. 9, pp. 2268–2272, 2008.

[26] S. Vijayaraghavan and D. Y. Goswami, "Photocatalytic oxidation of toluene in water from an algae pond with high dissolved oxygen content," *Journal of Solar Energy Engineering, Transactions of the ASME*, vol. 125, no. 2, pp. 230–232, 2003.

[27] D. Y. Goswami, D. M. Trivedi, and S. S. Block, "Photocatalytic disinfection of indoor air," *Journal of Solar Energy Engineering, Transactions of the ASME*, vol. 119, no. 1, pp. 92–96, 1997.

[28] S. Baruah, M. Abbas, M. Myint, T. Bora, and J. Dutta, "Enhanced visible light photocatalysis through fast crystallization of zinc oxide nanorods," *Beilstein Journal of Nanotechnology*, vol. 1, pp. 14–20, 2010.

[29] S. Rehman, R. Ullah, A. M. Butt, and N. D. Gohar, "Strategies of making TiO_2 and ZnO visible light active," *Journal of Hazardous Materials*, vol. 170, no. 2-3, pp. 560–569, 2009.

[30] S. Ahmed, M. G. Rasul, W. N. Martens, R. Brown, and M. A. Hashib, "Heterogeneous photocatalytic degradation of phenols in wastewater: a review on current status and developments," *Desalination*, vol. 261, no. 1-2, pp. 3–18, 2010.

[31] S. Linic, P. Christopher, and D. Ingram, "Plasminic-metal nanostructures for efficient conversion of solar to chemical energy," *Nature Materials*, vol. 10, pp. 911–921, 2011.

[32] S.S. Srinivasan, J. Wade, and E.K. Stefanakos, "Synthesis and characterization of photocatalytic TiO2-$ZnFe_2O_4$ nanoparticles," *Journal of Nanomaterials*, vol. 2006, Article ID 45712, 4 pages, 2006.

[33] D. S. Bhatkhande, V. G. Pangarkar, and A. A. C. M. Beenackers, "Photocatalytic degradation for environmental applications—a review," *Journal of Chemical Technology and Biotechnology*, vol. 77, no. 1, pp. 102–116, 2002.

[34] A. Alkauskas and A. Pasquarello, "Band-edge problem in the theoretical determination of defect energy levels: the O vacancy in ZnO as a benchmark case," *Physical Review B*, vol. 84, Article ID 125206, 11 pages, 2011.

[35] M. Ladanov, M. K. Ram, G. Matthews, and A. Kumar, "Structure and opto-electrochemical properties of ZnO nanowires grown on n-Si substrate," *Langmuir*, vol. 27, no. 14, pp. 9012–9017, 2011.

[36] D. M. Fouad and M. B. Mohamed, "Comparative study of the photocatalytic activity of semiconductor nanostructures and their hybrid metal nanocomposites on the photodegradation of malathion," *Journal of Nanomaterials*, vol. 2012, Article ID 524123, 8 pages, 2012.

[37] A. A. Khodja, T. Sehili, J. F. Pilichowski, and P. Boule, "Photocatalytic degradation of 2-phenylphenol on TiO_2 and ZnO in aqueous suspensions," *Journal of Photochemistry and Photobiology A*, vol. 141, no. 2-3, pp. 231–239, 2001.

[38] G. Marcì, V. Augugliaro, M. J. López-Muñoz et al., "Preparation characterization and photocatalytic activity of polycrystalline ZnO/TiO_2 systems. 2. Surface, bulk characterization, and 4-nitrophenol photodegradation in liquid-solid regime," *Journal of Physical Chemistry B*, vol. 105, no. 5, pp. 1033–1040, 2001.

[39] N. Sobana and M. Swaminathan, "The effect of operational parameters on the photocatalytic degradation of acid red 18 by ZnO," *Separation and Purification Technology*, vol. 56, no. 1, pp. 101–107, 2007.

[40] Q. Wan, T. H. Wang, and J. C. Zhao, "Enhanced photocatalytic activity of ZnO nanotetrapods," *Applied Physics Letters*, vol. 87, no. 8, pp. 1–3, 2005.

[41] N. V. Kaneva, D. T. Dimitrov, and C. D. Dushkin, "Effect of nickel doping on the photocatalytic activity of ZnO thin films under UV and visible light," *Applied Surface Science*, vol. 257, no. 18, pp. 8113–8120, 2011.

[42] S. Sakthivel, B. Neppolian, M. V. Shankar, B. Arabindoo, M. Palanichamy, and V. Murugesan, "Solar photocatalytic degradation of azo dye: comparison of photocatalytic efficiency of ZnO and TiO_2," *Solar Energy Materials and Solar Cells*, vol. 77, no. 1, pp. 65–82, 2003.

[43] S. Linic, P. Christopher, and D. Ingram, "Plasmonic-metal nanostructures for efficient conversion of solar to chemical energy," *Nature Materials*, vol. 10, pp. 911–921, 2011.

[44] S. Baruah, F. F. Rafique, and J. Dutta, "Visible light photocatalysis by tailoring crystal defections in zinc oxide nanostructures," *Nano*, vol. 3, no. 5, pp. 399–407, 2008.

[45] S. Baruah and J. Dutta, "pH-dependent growth of zinc oxide nanorods," *Journal of Crystal Growth*, vol. 311, no. 8, pp. 2549–2554, 2009.

[46] Z. Zhang and J. Mu, "Hydrothermal synthesis of ZnO nanobundles controlled by PEO-PPO-PEO block copolymers," *Journal of Colloid and Interface Science*, vol. 307, no. 1, pp. 79–82, 2007.

[47] E. W. Petersen, E. M. Likovich, K. J. Russell, and V. Narayanamurti, "Growth of ZnO nanowires catalyzed by size-dependent melting of Au nanoparticles," *Nanotechnology*, vol. 20, no. 40, Article ID 405603, 2009.

[48] L. N. Protasova, E. V. Rebrov, K. L. Choy et al., "ZnO based nanowires grown by chemical vapour deposition for selective hydrogenation of acetylene alcohols," *Catalysis Science and Technology*, vol. 1, no. 5, pp. 768–777, 2011.

[49] S. Ashraf, A. C. Jones, J. Bacsa et al., "MOCVD of vertically aligned ZnO nanowires using bidentate ether adducts of dimethylzinc," *Chemical Vapor Deposition*, vol. 17, no. 1–3, pp. 45–53, 2011.

[50] L. Wang, X. Zhang, S. Zhao, G. Zhou, Y. Zhou, and J. Qi, "Synthesis of well-aligned ZnO nanowires by simple physical vapor deposition on c-oriented ZnO thin films without catalysts or additives," *Applied Physics Letters*, vol. 86, no. 2, Article ID 024108, 2005.

[51] J. S. Wang, C. S. Yang, P. I. Chen et al., "Catalyst-free highly vertically aligned ZnO nanoneedle arrays grown by plasma-assisted molecular beam epitaxy," *Applied Physics A*, vol. 97, no. 3, pp. 553–557, 2009.

[52] L. C. Tien, S. J. Pearton, D. P. Norton, and F. Ren, "Synthesis and microstructure of vertically aligned ZnO nanowires grown by high-pressure-assisted pulsed-laser deposition," *Journal of Materials Science*, vol. 43, no. 21, pp. 6925–6932, 2008.

[53] K. Kitamura, T. Yatsui, M. Ohtsu, and G. C. Yi, "Fabrication of vertically aligned ultrafine ZnO nanorods using metal-organic vapor phase epitaxy with a two-temperature growth method," *Nanotechnology*, vol. 19, no. 17, Article ID 175305, 2008.

[54] D. I. Suh, C. C. Byeon, and C. L. Lee, "Synthesis and optical characterization of vertically grown ZnO nanowires in high crystallinity through vapor-liquid-solid growth mechanism," *Applied Surface Science*, vol. 257, no. 5, pp. 1454–1456, 2010.

[55] X. Wang, J. Song, P. Li et al., "Growth of uniformly aligned ZnO nanowire heterojunction arrays on GaN, AlN, and $Al_{0.5}Ga_{0.5}N$ substrates," *Journal of the American Chemical Society*, vol. 127, no. 21, pp. 7920–7923, 2005.

[56] J. Song, X. Wang, E. Riedo, and Z. L. Wang, "Systematic study on experimental conditions for large-scale growth of aligned ZnO nanwires on nitrides," *Journal of Physical Chemistry B*, vol. 109, no. 20, pp. 9869–9872, 2005.

[57] X. Wang, J. Song, C. J. Summers et al., "Density-controlled growth of aligned ZnO nanowires sharing a common contact: a simple, low-cost, and mask-free technique for large-scale applications," *Journal of Physical Chemistry B*, vol. 110, no. 15, pp. 7720–7724, 2006.

[58] F.-H. Chu, C.-W. Huang, C.-L. Hsin et al., "Well-aligned ZnO nanowires with excellent field emission and photocatalytic properties," *Nanoscale*, vol. 4, pp. 1471–1475, 2012.

[59] S. Ashraf, A. C. Jones, J. Bacsa et al., "MOCVD of vertically aligned ZnO nanowires using bidentate ether adducts of dimethylzinc," *Chemical Vapor Deposition*, vol. 17, no. 1–3, pp. 45–53, 2011.

[60] M. H. Huang, Y. Y. Wu, H. Feick, N. Tran, E. Weber, and P. D. Yang, "Catalytic growth of zinc oxide nanowires by vapor transport," *Advanced Materials*, vol. 13, pp. 113–116, 2001.

[61] Y. J. Zeng, Z. Z. Ye, W. Z. Xu, L. P. Zhu, and B. H. Zhao, "Well-aligned ZnO nanowires grown on Si substrate via metal-organic chemical vapor deposition," *Applied Surface Science*, vol. 250, no. 1–4, pp. 280–283, 2005.

[62] B. Zhang, S. Zhou, B. Liu, H. Gong, and X. Zhang, "Fabrication and green emission of ZnO nanowire arrays," *Science in China, Series E*, vol. 52, no. 4, pp. 883–887, 2009.

[63] B. Liu and H. C. Zeng, "Hydrothermal synthesis of ZnO nanorods in the diameter regime of 50 nm," *Journal of the American Chemical Society*, vol. 125, no. 15, pp. 4430–4431, 2003.

[64] G. An, Z. Sun, Y. Zhang et al., "CO_2-mediated synthesis of ZnO nanorods and their application in sensing ethanol vapor," *Journal of Nanoscience and Nanotechnology*, vol. 11, pp. 1252–1258, 2011.

[65] J. Y. Kim, J. W. Cho, and S. H. Kim, "The characteristic of the ZnO nanowire morphology grown by the hydrothermal method on various surface-treated seed layers," *Materials Letters*, vol. 65, no. 8, pp. 1161–1164, 2011.

[66] J. Song, S. Baek, H. Lee, and S. Lim, "Selective growth of vertical zno nanowires with the control of hydrothermal synthesis and nano-lmprint technology," *Journal of Nanoscience and Nanotechnology*, vol. 9, no. 6, pp. 3909–3913, 2009.

[67] S. Baruah and J. Dutta, "Hydrothermal growth of ZnO nanostructures," *Science and Technology of Advanced Materials*, vol. 10, no. 1, Article ID 013001, 2009.

[68] A. Sugunan, H. C. Warad, M. Boman, and J. Dutta, "Zinc oxide nanowires in chemical bath on seeded substrates: role of hexamine," *Journal of Sol-Gel Science and Technology*, vol. 39, no. 1, pp. 49–56, 2006.

[69] S. Xu, C. Lao, B. Weintraub, and Z. L. Wang, "Density-controlled growth of aligned ZnO nanowire arrays by seedles chemical approach on smooth surfaces," *Journal of Materials Research*, vol. 23, no. 8, pp. 2072–2077, 2008.

[70] L. E. Greene, M. Law, D. H. Tan et al., "General route to vertical ZnO nanowire arrays using textured ZnO seeds," *Nano Letters*, vol. 5, no. 7, pp. 1231–1236, 2005.

[71] S. Baruah and J. Dutta, "Effect of seeded substrates on hydrothermally grown ZnO nanorods," *Journal of Sol-Gel Science and Technology*, vol. 50, no. 3, pp. 456–464, 2009.

[72] H. Ghayour, H. R. Rezaie, S. Mirdamadi, and A. A. Nourbakhsh, "The effect of seed layer thickness on alignment and morphology of ZnO nanorods," *Vacuum*, vol. 86, no. 1, pp. 101–105, 2011.

[73] W. Y. Wu, C. C. Yeh, and J. M. Ting, "Effects of seed layer characteristics on the synthesis of ZnO nanowires," *Journal of the American Ceramic Society*, vol. 92, no. 11, pp. 2718–2723, 2009.

[74] G. Kenanakis, D. Vernardou, E. Koudoumas, and N. Katsarakis, "Growth of c-axis oriented ZnO nanowires from aqueous solution: the decisive role of a seed layer for controlling the wires' diameter," *Journal of Crystal Growth*, vol. 311, no. 23-24, pp. 4799–4804, 2009.

[75] L. W. Ji, S. M. Peng, J. S. Wu, W. S. Shih, C. Z. Wu, and I. T. Tang, "Effect of seed layer on the growth of well-aligned ZnO nanowires," *Journal of Physics and Chemistry of Solids*, vol. 70, no. 10, pp. 1359–1362, 2009.

[76] J. H. Tian, J. Hu, S. S. Li et al., "Improved seedless hydrothermal synthesis of dense and ultralong ZnO nanowires," *Nanotechnology*, vol. 22, no. 24, Article ID 245601, 2011.

[77] T. Al-Harbi, "Hydrothermal synthesis and optical properties of Ni doped ZnO hexagonal nanodiscs," *Journal of Alloys and Compounds*, vol. 509, no. 2, pp. 387–390, 2011.

[78] J. Wang and L. Gao, "Wet chemical synthesis of ultralong and straight single-crystalline ZnO nanowires and their excellent UV emission properties," *Journal of Materials Chemistry*, vol. 13, no. 10, pp. 2551–2554, 2003.

[79] L. Gong, X. Wu, H. Chen, F. Qu, and M. An, "Synthesis of vertically aligned dense ZnO nanowires," *Journal of Nanomaterials*, vol. 2011, Article ID 428172, 5 pages, 2011.

[80] H. Hu, X. Huang, C. Deng, X. Chen, and Y. Qian, "Hydrothermal synthesis of ZnO nanowires and nanobelts on a large scale," *Materials Chemistry and Physics*, vol. 106, no. 1, pp. 58–62, 2007.

[81] K. Govender, D. S. Boyle, P. B. Kenway, and P. O'Brien, "Understanding the factors that govern the deposition and morphology of thin films of ZnO from aqueous solution?" *Journal of Materials Chemistry*, vol. 14, no. 16, pp. 2575–2591, 2004.

[82] M. N. R. Ashfold, R. P. Doherty, N. G. Ndifor-Angwafor, D. J. Riley, and Y. Sun, "The kinetics of the hydrothermal growth of ZnO nanostructures," *Thin Solid Films*, vol. 515, no. 24, pp. 8679–8683, 2007.

[83] S. F. Wang, T. Y. Tseng, Y. R. Wang, C. Y. Wang, H. C. Lu, and W. L. Shih, "Effects of preparation conditions on the growth of ZnO nanorod arrays using aqueous solution method," *International Journal of Applied Ceramic Technology*, vol. 5, no. 5, pp. 419–429, 2008.

[84] A. R. Kim, J.-Y. Lee, B. R. Jang, J. Y. Lee, H. S. Kim, and N. W. Jang, "Effect of Zn^{2+} source concentration on hydrothermally grown ZnO nanorods," *Journal of Nanoscience and Nanotechnology*, vol. 11, pp. 6395–6399, 2011.

[85] Z. Yuan, J. Yu, N. Wang, and Y. Jiang, "Well-aligned ZnO nanorod arrays from diameter-controlled growth and their application in inverted polymer solar cell," *Journal of Materials Science*, vol. 12, pp. 502–507, 2011.

[86] M. Law, L. E. Greene, J. C. Johnson, R. Saykally, and P. Yang, "Nanowire dye-sensitized solar cells," *Nature Materials*, vol. 4, no. 6, pp. 455–459, 2005.

[87] S. H. Ko, D. Lee, H. W. Kang et al., "Nanoforest of hydrothermally grown hierarchical ZnO nanowires for a high efficiency dye-sensitized solar cell," *Nano Letters*, vol. 11, no. 2, pp. 666–671, 2011.

[88] O. Akhavan, M. Mehrabian, K. Mirabbaszadeh, and R. Azimirad, "Hydrothermal synthesis of ZnO nanorod arrays for photocatalytic inactivation of bacteria," *Journal of Physics D*, vol. 42, no. 22, Article ID 225305, 2009.

[89] M. K. Kim, D. K. Yi, and U. Paik, "Tunable, flexible antireflection layer of ZnO nanowires embedded in PDMS," *Langmuir*, vol. 26, no. 10, pp. 7552–7554, 2010.

[90] L. Li, T. Zhai, H. Zeng, X. Fang, Y. Bando, and D. Golberg, "Polystyrene sphere-assisted one-dimensional nanostructure arrays: synthesis and applications," *Journal of Materials Chemistry*, vol. 21, no. 1, pp. 40–56, 2011.

[91] C. Y. Lee, S. Y. Li, P. Lin, and T. Y. Tseng, "ZnO nanowires hydrothermally grown on PET polymer substrates and their characteristics," *Journal of Nanoscience and Nanotechnology*, vol. 5, no. 7, pp. 1088–1094, 2005.

[92] S. Baruah, C. Thanachayanont, and J. Dutta, "Growth of ZnO nanowires on nonwoven polyethylene fibers," *Science*

and Technology of Advanced Materials, vol. 9, no. 2, Article ID 025009, 2008.

[93] Y. Qin, X. Wang, and Z. L. Wang, "Microfibre-nanowire hybrid structure for energy scavenging," *Nature*, vol. 451, no. 7180, pp. 809–813, 2008.

[94] T. Y. Liu, H. C. Liao, C. C. Lin, S. H. Hu, and S. Y. Chen, "Biofunctional ZnO nanorod arrays grown on flexible substrates," *Langmuir*, vol. 22, no. 13, pp. 5804–5809, 2006.

[95] H. Ahn, J. H. Park, S. B. Kim, S. H. Jee, Y. S. Yoon, and D. J. Kim, "Vertically aligned zno nanorod sensor on flexible substrate for ethanol gas monitoring," *Electrochemical and Solid-State Letters*, vol. 13, no. 11, pp. J125–J128, 2010.

[96] S. Baruah, M. Jaisai, R. Imani, M. M. Nazhad, and J. Dutta, "Photocatalytic paper using zinc oxide nanorods," *Science and Technology of Advanced Materials*, vol. 11, no. 5, Article ID 055002, 2010.

[97] M. Afsal and L.-J. Chen, "Anomalous adhesive superhydrophobicity on aligned ZnO nanowire arrays grown on a lotus leaf," *Journal of Materials Chemistry*, vol. 21, pp. 18061–18066, 2011.

[98] Y. Zhou, W. Wu, G. Hu, H. Wu, and S. Cui, "Hydrothermal synthesis of ZnO nanorod arrays with the addition of polyethyleneimine," *Materials Research Bulletin*, vol. 43, no. 8-9, pp. 2113–2118, 2008.

[99] L.-Y. Chen, Y.-T. Yin, C.-H. Chen, and J.-W. Chiou, "Influence of polyethyleneimine and ammonium on the growth of ZnO nanowires by hydrothermal method," *Journal of Physical Chemistry C*, vol. 115, pp. 20913–20919, 2011.

[100] J. J. Hassan, Z. Hassan, and H. Abu-Hassan, "High-quality vertically aligned ZnO nanorods synthesized by microwave-assisted CBD with ZnO-PVA complex seed layer on Si substrates," *Journal of Alloys and Compounds*, vol. 509, no. 23, pp. 6711–6719, 2011.

[101] L. Zhang and Y. J. Zhu, "ZnO micro- and nano-structures: microwave-assisted solvothermal synthesis, morphology control and photocatalytic properties," *Applied Physics A*, vol. 97, no. 4, pp. 847–852, 2009.

[102] H. E. Unalan, P. Hiralal, N. Rupesinghe, S. Dalal, W. I. Milne, and G. A. J. Amaratunga, "Rapid synthesis of aligned zinc oxide nanowires," *Nanotechnology*, vol. 19, no. 25, Article ID 255608, 2008.

[103] S. K. Lim, S. H. Hwang, and S. Kim, "Microemulsion synthesis and characterization of aluminum doped ZnO nanorods," *Crystal Research and Technology*, vol. 45, no. 7, pp. 771–775, 2010.

[104] J. Jiang, Y. Li, S. Tan, and Z. Huang, "Synthesis of zinc oxide nanotetrapods by a novel fast microemulsion-based hydrothermal method," *Materials Letters*, vol. 64, no. 20, pp. 2191–2193, 2010.

[105] C. Wu, L. Shen, H. Yu, Q. Huang, and Y. C. Zhang, "Synthesis of Sn-doped ZnO nanorods and their photocatalytic properties," *Materials Research Bulletin*, vol. 46, no. 7, pp. 1107–1112, 2011.

[106] W. Baiqi, S. Xudong, F. Qiang et al., "Photoluminescence properties of Co-doped ZnO nanorods array fabricated by the solution method," *Physica E*, vol. 41, no. 3, pp. 413–417, 2009.

[107] D. Li, L. Zhao, R. Wu, C. Ronning, and J. G. Lu, "Temperature-dependent photoconductance of heavily doped ZnO nanowires," *Nano Research*, vol. 4, pp. 1110–1116, 2011.

[108] D. Wang, G. Xing, M. Gao, L. Yang, J. Yang, and T. Wu, "Defects-mediated energy transfer in red-light-emitting Eu-doped ZnO nanowire arrays," *Journal of Physical Chemistry C*, vol. 115, pp. 22729–22735, 2011.

[109] K. P. Kim, D. Chang, S. K. Lim, S. K. Lee, H. K. Lyu, and D. K. Hwang, "Thermal annealing effects on the dynamic photoresponse properties of Al-doped ZnO nanowires network," *Current Applied Physics*, vol. 11, pp. 1311–1314, 2011.

[110] T. Kataoka, Y. Yamazaki, V. R. Singh et al., "Ferromagnetic interaction between Cu ions in the bulk region of Cu-doped ZnO nanowires," *Physical Review B*, vol. 84, Article ID 153203, 4 pages, 2011.

[111] Z. Dai, A. Nurbawono, A. Zhang et al., "C-doped ZnO nanowires: electronic structures, magnetic properties, and a possible spintronic device," *Journal of Chemical Physics*, vol. 134, no. 10, Article ID 104706, 2011.

[112] H. Xu, A. L. Rosa, T. Frauenheim, and R. Q. Zhang, "N-doped ZnO nanowires: surface segregation, the effect of hydrogen passivation and applications in spintronics," *Physica Status Solidi B*, vol. 247, no. 9, pp. 2195–2201, 2010.

[113] J. Gao, Q. Zhao, Y. Sun, G. Li, J. Zhang, and D. Yu, "A novel way for synthesizing phosphorus-doped ZnO nanowires," *Nanoscale Research Letters*, vol. 6, no. 1, pp. 1–6, 2011.

[114] J. Fan, A. Shavel, R. Zamani et al., "Control of the doping concentration, morphology and optoelectronic properties of vertically aligned chlorine-doped ZnO nanowires," *Acta Materialia*, vol. 59, pp. 6790–6800, 2011.

[115] H. Li, Y. Huang, Q. Zhang et al., "Facile synthesis of highly uniform Mn/Co-codoped ZnO nanowires: optical, electrical, and magnetic properties," *Nanoscale*, vol. 3, no. 2, pp. 654–660, 2011.

[116] C. W. Zou, L. X. Shao, L. P. Guo, D. J. Fu, and T. W. Kang, "Ferromagnetism and ferroelectric properties of (Mn, Li) co-doped ZnO nanorods arrays deposited by electrodeposition," *Journal of Crystal Growth*, vol. 331, pp. 44–48, 2011.

[117] S. N. Das, J. H. Choi, J. P. Kar, T. I. Lee, and J. M. Myoung, "Fabrication of p-type ZnO nanowires based heterojunction diode," *Materials Chemistry and Physics*, vol. 121, no. 3, pp. 472–476, 2010.

[118] D. Li, Z. T. Liu, Y. H. Leung, A. B. Djurišić, M. H. Xie, and W. K. Chan, "Transition metal-doped ZnO nanorods synthesized by chemical methods," *Journal of Physics and Chemistry of Solids*, vol. 69, no. 2-3, pp. 616–619, 2008.

[119] A. Marzouki, F. Falyouni, N. Haneche et al., "Structural and optical characterizations of nitrogen-doped ZnO nanowires grown by MOCVD," *Materials Letters*, vol. 64, no. 19, pp. 2112–2114, 2010.

[120] A. Escobedo Morales, M. Herrera Zaldivar, and U. Pal, "Indium doping in nanostructured ZnO through low-temperature hydrothermal process," *Optical Materials*, vol. 29, no. 1, pp. 100–104, 2006.

[121] T. H. Fang and S. H. Kang, "Optical and physical characteristics of In-doped ZnO nanorods," *Current Applied Physics*, vol. 10, no. 4, pp. 1076–1086, 2010.

[122] C. Ren, B. Yang, M. Wu et al., "Synthesis of Ag/ZnO nanorods array with enhanced photocatalytic performance," *Journal of Hazardous Materials*, vol. 182, no. 1–3, pp. 123–129, 2010.

[123] Y. Zhang, M. K. Ram, E. K. Stefanakos, and D. Y. Goswami, "Enhanced photocatalytic activity of ZnO/Fe nanowires for water decontamination," In press.

[124] O. Lupan, V. M. Guérin, I. M. Tiginyanu et al., "Well-aligned arrays of vertically oriented ZnO nanowires electrodeposited on ITO-coated glass and their integration in dye sensitized solar cells," *Journal of Photochemistry and Photobiology A*, vol. 211, no. 1, pp. 65–73, 2010.

[125] A. P. de Moura, R. C. Lima, M. L. Moreira et al., "ZnO architectures synthesized by a microwave-assisted hydrothermal

method and their photoluminescence properties," *Solid State Ionics*, vol. 181, no. 15-16, pp. 775–780, 2010.

[126] G. Nagaraju, S. Ashoka, P. Chithaiah, C. N. Tharamani, and G. T. Chandrappa, "Surfactant free hydrothermally derived ZnO nanowires, nanorods, microrods and their characterization," *Materials Science in Semiconductor Processing*, vol. 13, no. 1, pp. 21–28, 2010.

[127] L. Li, H. Yang, H. Zhao et al., "Hydrothermal synthesis and gas sensing properties of single-crystalline ultralong ZnO nanowires," *Applied Physics A*, vol. 98, no. 3, pp. 635–641, 2010.

[128] V. P. Verma, S. Das, S. Hwang, H. Choi, M. Jeon, and W. Choi, "Nitric oxide gas sensing at room temperature by functionalized single zinc oxide nanowire," *Materials Science and Engineering B*, vol. 171, no. 1–3, pp. 45–49, 2010.

[129] C. W. Na, H. S. Woo, I. D. Kim, and J. H. Lee, "Selective detection of NO_2 and C_2H_5OH using a CO_3O_4-decorated ZnO nanowire network sensor," *Chemical Communications*, vol. 47, no. 18, pp. 5148–5150, 2011.

[130] J. Y. Park, Y. K. Park, and S. S. Kim, "Formation of networked ZnO nanowires by vapor phase growth and their sensing properties with respect to CO," *Materials Letters*, vol. 65, no. 17-18, pp. 2755–2757, 2011.

[131] I. C. Yao, P. Lin, and T. Y. Tseng, "Hydrogen gas sensors using ZnO-SNO_2 core-shell nanostructure," *Advanced Science Letters*, vol. 3, no. 4, pp. 548–553, 2010.

[132] N. Mohseni Kiasari and P. Servati, "Dielectrophoresis-assembled ZnO nanowire oxygen sensors," *IEEE Electron Device Letters*, vol. 32, no. 7, pp. 982–984, 2011.

[133] X. Zhou, J. Li, M. Ma, and Q. Xue, "Effect of ethanol gas on the electrical properties of ZnO nanorods," *Physica E*, vol. 43, no. 5, pp. 1056–1060, 2011.

[134] E. Oh, H. Y. Choi, S. H. Jung et al., "High-performance NO_2 gas sensor based on ZnO nanorod grown by ultrasonic irradiation," *Sensors and Actuators, B*, vol. 141, no. 1, pp. 239–243, 2009.

[135] A. Wei, Z. Wang, L.-H. Pan et al., "Room-temperature NH_3 gas sensor based on hydrothermally grown ZnO nanorods," *Chinese Physics Letters*, vol. 28, no. 8, Article ID 080702, 2011.

[136] E. Oh and S. H. Jeong, "Sonochemical method for fabricating a high-performance ZnO nanorod sensor for CO gas detection," *Journal of the Korean Physical Society*, vol. 59, no. 1, pp. 8–11, 2011.

[137] A. Fulati, S. M. U. Ali, M. H. Asif et al., "An intracellular glucose biosensor based on nanoflake ZnO," *Sensors and Actuators, B*, vol. 150, no. 2, pp. 673–680, 2010.

[138] S. M. Usman Ali, O. Nur, M. Willander, and B. Danielsson, "Glucose detection with a commercial MOSFET using a ZnO nanowires extended gate," *IEEE Transactions on Nanotechnology*, vol. 8, no. 6, pp. 678–683, 2009.

[139] X. Liu, Q. Hu, Q. Wu, W. Zhang, Z. Fang, and Q. Xie, "Aligned ZnO nanorods: a useful film to fabricate amperometric glucose biosensor," *Colloids and Surfaces B*, vol. 74, no. 1, pp. 154–158, 2009.

[140] Z. H. Ibupoto, S. M. Ali, K. Khun, C. Chey, O. Nur, and M. Willander, "ZnO nanorods based enzymatic biosensor for selective determination of penicillin," *Biosensors*, vol. 1, pp. 153–163, 2011.

[141] A. Choi, K. Kim, H. I. Jung, and S. Y. Lee, "ZnO nanowire biosensors for detection of biomolecular interactions in enhancement mode," *Sensors and Actuators, B*, vol. 148, no. 2, pp. 577–582, 2010.

[142] C. Y. Lu, S. P. Chang, S. J. Chang et al., "A lateral ZnO nanowire UV photodetector prepared on a ZnO:Ga/glass template," *Semiconductor Science and Technology*, vol. 24, no. 7, Article ID 075005, 2009.

[143] K. J. Chen, F. Y. Hung, S. J. Chang, and S. J. Young, "Optoelectronic characteristics of UV photodetector based on ZnO nanowire thin films," *Journal of Alloys and Compounds*, vol. 479, no. 1-2, pp. 674–677, 2009.

[144] F. Fang, J. Futter, A. Markwitz, and J. Kennedy, "UV and humidity sensing properties of ZnO nanorods prepared by the arc discharge method," *Nanotechnology*, vol. 20, no. 24, Article ID 245502, 2009.

[145] Y. Li, F. D. Valle, M. Simonnet, I. Yamada, and J. J. Delaunay, "High-performance UV detector made of ultra-long ZnO bridging nanowires," *Nanotechnology*, vol. 20, no. 4, Article ID 045501, 2009.

[146] P. Y. Yang, J. L. Wang, W. C. Tsai et al., "Photoresponse of hydrothermally grown lateral ZnO nanowires," *Thin Solid Films*, vol. 518, no. 24, pp. 7328–7332, 2010.

[147] D. Lin, H. Wu, W. Zhang, H. Li, and W. Pan, "Enhanced UV photoresponse from heterostructured Ag-ZnO nanowires," *Applied Physics Letters*, vol. 94, no. 17, Article ID 172103, 2009.

[148] H. Chang, Z. Sun, K. Y. F. Ho et al., "A highly sensitive ultraviolet sensor based on a facile in situ solution-grown ZnO nanorod/graphene heterostructure," *Nanoscale*, vol. 3, no. 1, pp. 258–264, 2011.

[149] M. H. Huang, S. Mao, H. Feick et al., "Room-temperature ultraviolet nanowire nanolasers," *Science*, vol. 292, no. 5523, pp. 1897–1899, 2001.

[150] R. Zhang, P. G. Yin, N. Wang, and L. Guo, "Photoluminescence and Raman scattering of ZnO nanorods," *Solid State Sciences*, vol. 11, no. 4, pp. 865–869, 2009.

[151] J. Zhong, H. Chen, G. Saraf et al., "Integrated ZnO nanotips on GaN light emitting diodes for enhanced emission efficiency," *Applied Physics Letters*, vol. 90, no. 20, Article ID 203515, 2007.

[152] C. H. Chen, S. J. Chang, S. P. Chang et al., "Electroluminescence from n-ZnO nanowires/p-GaN heterostructure light-emitting diodes," *Applied Physics Letters*, vol. 95, no. 22, Article ID 223101, 2009.

[153] X. M. Zhang, M. Y. Lu, Y. Zhang, L. J. Chen, and Z. L. Wang, "Fabrication of a high-brightness blue-light-emitting diode using a ZnO-Nanowire array grown on p-GaN thin film," *Advanced Materials*, vol. 21, no. 27, pp. 2767–2770, 2009.

[154] X. W. Sun, B. Ling, J. L. Zhao et al., "Ultraviolet emission from a ZnO rod homojunction light-emitting diode," *Applied Physics Letters*, vol. 95, no. 13, Article ID 133124, 2009.

[155] Q. Zhang, C. S. Dandeneau, X. Zhou, and C. Cao, "ZnO nanostructures for dye-sensitized solar cells," *Advanced Materials*, vol. 21, no. 41, pp. 4087–4108, 2009.

[156] H. M. Cheng, W. H. Chiu, C. H. Lee, S. Y. Tsai, and W. F. Hsieh, "Formation of branched ZnO nanowires from solvothermal method and dye-sensitized solar cells applications," *Journal of Physical Chemistry C*, vol. 112, no. 42, pp. 16359–16364, 2008.

[157] G. Zhu, R. Yang, S. Wang, and Z. L. Wang, "Flexible high-output nanogenerator based on lateral ZnO nanowire array," *Nano Letters*, vol. 10, no. 8, pp. 3151–3155, 2010.

[158] A. Sugunan, V. K. Guduru, A. Uheida, M. S. Toprak, and M. Muhammed, "Radially oriented ZnO nanowires on flexible poly-L-lactide nanofibers for continuous-flow photocatalytic water purification," *Journal of the American Ceramic Society*, vol. 93, no. 11, pp. 3740–3744, 2010.

[159] Z. L. Wang and J. Song, "Piezoelectric nanogenerators based on zinc oxide nanowire arrays," *Science*, vol. 312, no. 5771, pp. 242–246, 2006.

[160] X. Wang, J. Song, J. Liu, and L. W. Zhong, "Direct-current nanogenerator driven by ultrasonic waves," *Science*, vol. 316, no. 5821, pp. 102–105, 2007.

[161] C. Chang, V. H. Tran, J. Wang, Y. K. Fuh, and L. Lin, "Direct-write piezoelectric polymeric nanogenerator with high energy conversion efficiency," *Nano Letters*, vol. 10, no. 2, pp. 726–731, 2010.

[162] S. Xu, Y. Qin, C. Xu, Y. Wei, R. Yang, and Z. L. Wang, "Self-powered nanowire devices," *Nature Nanotechnology*, vol. 5, no. 5, pp. 366–373, 2010.

[163] Y. Hu, C. Xu, Y. Zhang, L. Lin, R. L. Snyder, and Z. L. Wang, "A Nanogenerator for energy harvesting from a rotating tire and its application as a self-powered pressure/speed sensor," *Advanced Materials*, vol. 23, pp. 4068–4071, 2011.

[164] C. Xu and Z. L. Wang, "Compact hybrid cell based on a convoluted nanowire structure for harvesting solar and mechanical energy," *Advanced Materials*, vol. 23, no. 7, pp. 873–877, 2011.

[165] S. N. Cha, J. S. Seo, S. M. Kim et al., "Sound-driven piezoelectric nanowire-based nanogenerators," *Advanced Materials*, vol. 22, no. 42, pp. 4726–4730, 2010.

[166] J. O. Hwang, D. H. Lee, J. Y. Kim et al., "Vertical ZnO nanowires/graphene hybrids for transparent and flexible field emission," *Journal of Materials Chemistry*, vol. 21, no. 10, pp. 3432–3437, 2011.

[167] Q. Zhao, C.-K. Huang, R. Zhu, J. Xu, L. Chen, and D. Yu, "2D planar field emission devices based on individual ZnO nanowires," *Solid State Communications*, vol. 151, pp. 1650–1653, 2011.

[168] H. W. Kang, J. Yeo, J. O. Hwang et al., "Simple ZnO nanowires patterned growth by microcontact printing for high performance field emission device," *Journal of Physical Chemistry C*, vol. 115, pp. 11435–11441, 2011.

[169] C. H. Chen, S. J. Chang, S. P. Chang et al., "Enhanced field emission of well-aligned ZnO nanowire arrays illuminated by UV," *Chemical Physics Letters*, vol. 490, no. 4–6, pp. 176–179, 2010.

[170] F. J. Sheini, M. A. More, S. R. Jadkar, K. R. Patil, V. K. Pillai, and D. S. Joag, "Observation of photoconductivity in Sn-Doped ZnO nanowires and their photoenhanced field emission behavior," *Journal of Physical Chemistry C*, vol. 114, no. 9, pp. 3843–3849, 2010.

[171] L. W. Chang, J. W. Yeh, C. L. Cheng, F. S. Shieu, and H. C. Shih, "Field emission and optical properties of Ga-doped ZnO nanowires synthesized via thermal evaporation," *Applied Surface Science*, vol. 257, no. 7, pp. 3145–3151, 2011.

[172] Z. Gao, J. Zhou, Y. Gu et al., "Effects of piezoelectric potential on the transport characteristics of metal-ZnO nanowire-metal field effect transistor," *Journal of Applied Physics*, vol. 105, no. 11, Article ID 113707, 2009.

[173] X. Wang, J. Zhou, J. Song, J. Liu, N. Xu, and Z. L. Wang, "Piezoelectric field effect transistor and nanoforce sensor based on a single ZnO nanowire," *Nano Letters*, vol. 6, no. 12, pp. 2768–2772, 2006.

[174] S. S. Kwon, W. K. Hong, G. Jo et al., "Piezoelectric effect on the electronic transport characteristics of ZnO nanowire field-effect transistors on bent flexible substrates," *Advanced Materials*, vol. 20, no. 23, pp. 4557–4562, 2008.

[175] P. Fei, P. H. Yeh, J. Zhou et al., "Piezoelectric potential gated field-effect transistor based on a free-standing ZnO wire," *Nano Letters*, vol. 9, no. 10, pp. 3435–3439, 2009.

[176] G. Kenanakis and N. Katsarakis, "Light-induced photocatalytic degradation of stearic acid by c-axis oriented ZnO nanowires," *Applied Catalysis A*, vol. 378, no. 2, pp. 227–233, 2010.

[177] Y. Zhang, J. Xu, P. Xu, Y. Zhu, X. Chen, and W. Yu, "Decoration of ZnO nanowires with Pt nanoparticles and their improved gas sensing and photocatalytic performance," *Nanotechnology*, vol. 21, no. 28, Article ID 285501, 2010.

[178] C. Ma, Z. Zhou, H. Wei, Z. Yang, Z. Wang, and Y. Zhang, "Rapid large-scale preparation of ZnO nanowires for photocatalytic application," *Nanoscale Research Letters*, vol. 6, no. 1, article 536, 2011.

[179] T. J. Kuo, C. N. Lin, C. L. Kuo, and M. H. Huang, "Growth of ultralong ZnO nanowires on silicon substrates by vapor transport and their use as recyclable photocatalysts," *Chemistry of Materials*, vol. 19, no. 21, pp. 5143–5147, 2007.

[180] Z. Zhu, D. Yang, and H. Liu, "Microwave-assisted hydrothermal synthesis of ZnO rod-assembled microspheres and their photocatalytic performances," *Advanced Powder Technology*, vol. 22, no. 4, pp. 493–497, 2011.

[181] K. Z. Zhang, B. Z. Lin, Y. L. Chen et al., "Fe-doped and ZnO-pillared titanates as visible-light-driven photocatalysts," *Journal of Colloid and Interface Science*, vol. 358, no. 2, pp. 360–368, 2011.

[182] C. Wu, L. Shen, Y. C. Zhang, and Q. Huang, "Solvothermal synthesis of Cr-doped ZnO nanowires with visible light-driven photocatalytic activity," *Materials Letters*, vol. 65, no. 12, pp. 1794–1796, 2011.

[183] Y. Lu, Y. Lin, D. Wang, L. Wang, T. Xie, and T. Jiang, "A high performance cobalt-doped ZnO visible light photocatalyst and its photogenerated charge transfer properties," *Nano Research*, vol. 4, pp. 1144–1152, 2011.

[184] T. Jia, W. Wang, F. Long, Z. Fu, H. Wang, and Q. Zhang, "Fabrication, characterization and photocatalytic activity of La-doped ZnO nanowires," *Journal of Alloys and Compounds*, vol. 484, no. 1-2, pp. 410–415, 2009.

[185] J. M. Wu, C. W. Fang, L. T. Lee et al., "Photoresponsive and ultraviolet to visible-light range photocatalytic properties of ZnO: Sb nanowires," *Journal of the Electrochemical Society*, vol. 158, no. 1, pp. K6–K10, 2011.

[186] M. A. Mahmood, S. Baruah, and J. Dutta, "Enhanced visible light photocatalysis by manganese doping or rapid crystallization with ZnO nanoparticles," *Materials Chemistry and Physics*, vol. 130, pp. 531–535, 2011.

[187] Y. Li, X. Zhao, and W. Fan, "Structural, electronic, and optical properties of Ag-doped ZnO nanowires: first principles study," *Journal of Physical Chemistry C*, vol. 115, no. 9, pp. 3552–3557, 2011.

[188] C. Wu and Q. Huang, "Synthesis of Na-doped ZnO nanowires and their photocatalytic properties," *Journal of Luminescence*, vol. 130, no. 11, pp. 2136–2141, 2010.

[189] S. Jung and K. Yong, "Fabrication of CuO-ZnO nanowires on a stainless steel mesh for highly efficient photocatalytic applications," *Chemical Communications*, vol. 47, no. 9, pp. 2643–2645, 2011.